Modeling the Release of CO_2 in the Deep Ocean

by

C. R. Liro, E. E. Adams, and H. J. Herzog

MIT-EL 91-002 June 1991

THE VIEWS EXPRESSED HEREIN ARE THE AUTHOR'S RESPONSIBILITY AND DO NOT NECESSARILY REFLECT THOSE OF THE MIT ENERGY LABORATORY OR THE MASSACHUSETTS INSTITUTE OF TECHNOLOGY.

Modeling the Release of CO_2 in the Deep Ocean

Final Report

by

Christopher R. Liro, E. Eric Adams, and Howard J. Herzog

Energy Laboratory
Massachusetts Institute of Technology
Cambridge, MA 02139

MIT-EL 91-002

June 1991

Prepared for: Mitsubishi Research Institute
Society and Technology Department
Tokyo, Japan

Acknowledgment

This research was funded by the Mitsubishi Research Institute, Society and Technology Department, Tokyo, Japan. That support is gratefully acknowledged.

Summary

The idea of capturing and disposing of carbon dioxide (CO_2) from the flue gas of fossil fuel-fired power plants has recently received attention as a possible mitigation strategy to counteract potential global warming due to the "greenhouse effect." One specific scheme is to concentrate the CO_2 in the flue gas to over 90 mol %, compress and dehydrate the CO_2 to supercritical conditions, and then transport it through a pipeline for deep ocean disposal. In Golomb *et al.* (1989), this scheme was studied, with emphasis on the CO_2 capture aspects. In this follow-on study, we concentrate on the mechanisms of releasing the CO_2 in the deep ocean.

Golomb *et al.* only considered the release of individual liquid CO_2 droplets in the region below 500 m. In this study, we consider all depths in both the liquid and vapor regions, and we model the entire plume in addition to individual droplets or bubbles. The key design variables in the model that can be controlled are: (1) release depth, (2) number of diffuser ports, N, and (3) initial bubble or droplet radius, r_o. The results show that we can lower the height of the plume by increasing the number of diffuser ports and/or decreasing the initial bubble or droplet radius. Figure S-1 summarizes the results for a release depth of 500 m. With reasonable values for N and r_o of 10 and 1 cm respectively, we can keep the plume height under 100 m. Since our goal is to dissolve all the CO_2 before it reaches the well-mixed surface layer at approximately 100 m, we can release our CO_2 at depths as shallow as 200 m. However, the residence time of the sequestered CO_2 in the ocean is also a function of depth. For releases of CO_2 less than 500 m deep, we can estimate a residence time of less than 50 years, and for a release from about 1000 m, a residence time from 200 to 300 years. These residence times may be increased by releasing in areas of downwelling or by forming

solid CO_2-hydrates which will sink to the ocean floor. For depths greater than 500 m, CO_2-hydrates may form but we have ignored them due to lack of data.

We estimate that the local CO_2 concentration will increase about 0.2 kg/m^3. Added to the background concentration of 0.1 kg/m^3, the resulting total concentration will be about 0.3 kg/m^3, much less than saturation levels of about 40 kg/m^3. Similarly, SO_2 and NO_x concentration increases will be about $1 \cdot 10^{-3}$ kg/m^3 and $2 \cdot 10^{-4}$ kg/m^3, respectively. Given an ambient current of 10 cm/s, horizontal dispersion will dilute these concentration increases by a factor of two at a distance of about 4 km downstream.

In implementing a CO_2 capture and sequester scheme based on an air separation/flue gas recycle power plant, the price of electricity would double. The reasons for this doubling are: (1) 44% due to derating of the power plant because of the parasitic power required to capture CO_2, mainly for air separation and CO_2 compression, (2) 42% due to capital charges and operation and maintenance costs (excluding fuel) of the power plant modifications, including air separation and CO_2 compression, and (3) 14% due to capital charges and operation and maintenance costs of a 160 km pipeline for deep ocean disposal. These numbers assume that no additional control measures are required to mitigate potential environmental problems are associated with deep ocean disposal of CO_2.

This study has advanced the state of knowledge concerning sequestering CO_2 in the deep ocean by modeling its release. However, serious questions still remain about the viability of the overall ocean disposal scheme due to potential environmental impacts and due to uncertainty of the residence time of the sequestered CO_2 in the ocean.

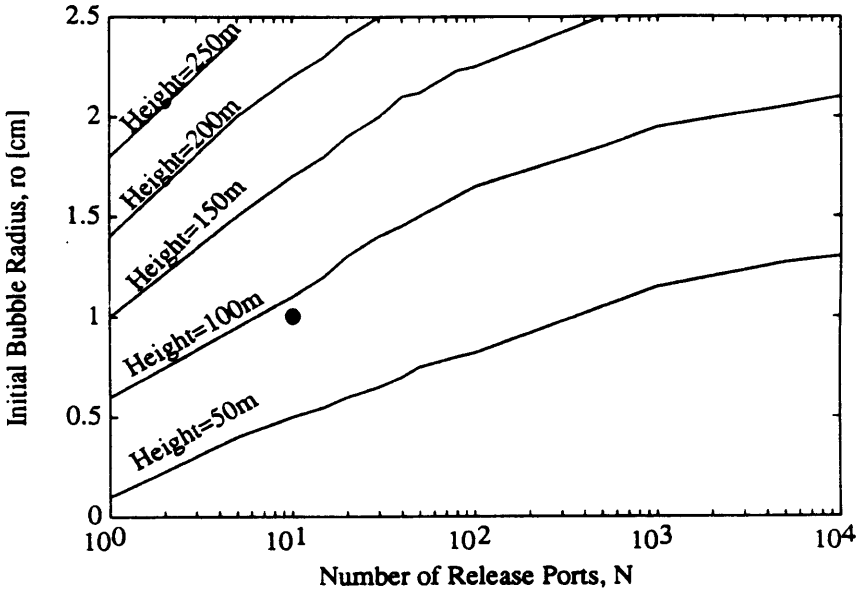

Figure S-1: Maximum plume height [m] as a function of initial bubble radius, r_o, and number of release ports, N, for a 500 m release depth. The sample case of r_o = 1.0 cm and N = 10 is marked in the figure.

Contents

List of Figures

List of Tables

Symbols

A	Projected frontal area of plume array
$\acute{A}$	Projected area of peeling portion of plume array
B	Buoyancy of plume
B_x	Average plume buoyancy at elevation x
B_w	Portion of plume buoyancy resulting from differences in water density
b	Nominal half width of plume
b_o	Initial value of b
C_d	Dissolved CO_2 concentration
C_s	Saturation value of C_d existing at the bubble or droplet interface
C_∞	Far-stream, ambient value of C_d
ΔC_d	Increase in C_d above normal ambient levels
$\Delta C_{d,m}$	Centerline increase in C_d above normal ambient levels
C	Concentration of CO_2 volume per unit plume volume
C_m	Centerline, maximum value of C
D	Diameter of release port
$\mathcal{D}$	Molecular diffusivity of CO_2 in water
d	Equivalent bubble or droplet diameter
g	Gravitational acceleration
K	Mass transfer coefficient
K_h	Equivalent eddy diffusivity coefficient for vertical thermocline transport

$L_{\frac{1}{2}}$	Horizontal distance over which concentrations will be diluted by a factor of two duo to horizontal dispersion
M	Plume momentum
$\dot{M}$	Rate of mass release of CO_2
N	Number of release ports in prototype diffuser
Q	Liquid volume flux
Q_e	Total entrained volume per plume length
q_{rel}	CO_2 volume flux at release depth
q_z	CO_2 volume flux at depth z
R	Radial distance from plume center
$\Re$	Bubble or droplet Reynold's number = dU_b/ν
r	Equivalent bubble or droplet diameter
r_z	Value of r at depth z
r_{max}	Maximum dynamically stable value of r
r_{rel}	Value of r at release depth
Sc	Molecular Schmidt number = $\nu/\mathcal{D}$
Sh	Sherwood number = $dK/\mathcal{D}$
T	Interfacial surface tension
t	Time
U_b	Terminal rise velocity, slip velocity of bubble or droplet
U	Local mean plume velocity
U_e	Entrainment velocity
U_m	Centerline, maximum value of mean plume velocity
$U_{m,o}$	Initial value of U_m
V_a	Ambient ocean current velocity
w	Lateral plume array width scale
x	Upward distance from plume origin
x_e	Upward distance to beginning of zone of established flow
x_o	Distance from virtual origin to beginning of established flow
Z_T	Depth of trapped CO_2

z	Ocean depth
z_o	Release depth
α	Entrainment coefficient
γ	Momentum amplification factor
λ_1	Spreading ratio of C to U
λ_2	Spreading ratio of $\Delta\rho_w$ to U
λ_d	Spreading ratio of C_d to U
ν	Viscocity of water
ρ	Local CO_2 density
ρ_a	Local density of ambient water
ρ_{rel}	Release density of CO_2
ρ_{mix}	Average density of the plume
ρ_{ref}	Reference density of water, taken as ambient density at release depth
ρ_w	Losal density of water within the plume
$\rho_{S,t,p}$	*In situ* density of seawater
$\rho_{S,t,0}$	Density of seawater at atmospheric pressure
$\Delta\rho_w$	Value of $\rho_w - \rho_a$
$\Delta\rho_{w,m}$	Centerline value of $\rho_w - \rho_a$
σ_t	Density difference with pure water at atmospheric pressure [g/cc]
$\sigma_{S,t,p}$	*In situ* density difference with pure water [g/cc]
$\mathcal{T}$	Time scale for CO_2 exchange to atmosphere

Chapter 1

Introduction

The ever-increasing use of fossil fuels worldwide is believed to be the principal cause of growth in the concentration of carbon dioxide (CO_2) in the earth's atmosphere. At present rates of emission, the CO_2 concentration is expected to double in the middle of the next century. Carbon dioxide is a "greenhouse gas" which absorbs infrared radiation leaving the earth and re-radiates it back down into the system. This effect may cause significant perturbations of the earth's radiative budget and consequently cause significant climatological and geohydrological changes. The exact impacts of the additional atmospheric CO_2 are still a subject of worldwide research. Efforts to decrease the emissions or mitigate the possible effects, however, are underway in a variety of countries, and it is likely that the future will bring further attention to addressing and acting on this problem.

1.1 Background

Fossil-fueled electric plants contribute about one-third of the world's CO_2 emissions from fossil-fuel sources, and generally, power plants have the highest density of CO_2 emissions in terms of mass per area per time. Thus these plants provide an appropriate focus as a control target.

The capture of CO_2 from the flue gas of fossil-fueled power plants is technically feasible, albeit it requires a significant fraction of the energy content of the fossil

fuel and additional equipment with large capital expenditures. This is because CO_2 typically constitutes only 10-15% by volume of the flue gas of fossil-fuel fired power plants. Most of the capture and disposal schemes, however, require the CO_2 to be concentrated to over 90% by volume. The captured CO_2 is envisioned to be liquefied at 150 atm, piped to the deep ocean, and released through a diffuser.

The capturing and sequestering of CO_2 in the ocean has been considered previously by several authors. Marchetti (1977) proposed collecting CO_2 and injecting it into the sea at the Strait of Gibraltar. Presumably, the current of denser Mediterranean water would carry it into the deep ocean where it would settle at a depth of about 1500 m. Other studies have proposed injecting liquid CO_2 at sufficient depths – about 3000 m – that the CO_2 would be more dense than the ambient sea water and would thus sink, or releasing it as a solid form, dry ice or CO_2-hydrate, which would sink to the bottom. Baes *et al.* (1980) proposed a process in which CO_2 would be mixed into solution with sea-water at a surface plant and then the denser by-product would be injected into the ocean where it would tend to sink. Steinberg *et al.* (1984, 1987) suggested the release of CO_2 gas at a depth of about 500 m. Albanese and Steinberg (1980) examined an ocean release in addition to several other disposal alternatives. Golomb *et al.* (1989) focused on liquid releases on the scale associated with a single plant, taking particular attention to examine the effects of the buoyancy of CO_2 recognizing that a release would tend to rise in the water column as the droplets went into solution.

Golomb *et al.* (1989) investigated five retrofit processes for capturing CO_2 from the flue gas of coal-fired power plants. They were (a) combustion of coal in an atmosphere of oxygen and recycled flue gas; (b) scrubbing the flue gas with monoethanolamine (MEA), a recyclable solvent; (c) cyrogenic CO_2 fractionation of the flue gas; (d) separation of CO_2 by selective membrane diffusion; and (e) scrubbing of the flue gas with sea water. The process that requires least incremental energy is air separation/flue gas recycling. In this process about 30% of the total energy content of the coal is consumed, and the thermal efficiency of a power plant is reduced from 35% to about 25%. Excluding pipeline and deep ocean disposal costs, it is estimated that the electricity

costs will increase by about 80%.

While these figures reflect retrofit options, increased efficiency may be achieved from new types of coal-fired power plants, specifically the Integrated Gasification Combined Cycle (IGCC) plant. For example, Smelser and Booras (1990) indicate that a 500 MW plant without disposal equipment could recover 90% of the CO_2 (as opposed to 100% for air separation/flue gas recycling) with a decrease in efficiency from 35% to 28.5% and with an electricity cost increase of 70%. A similar study by Hendriks *et al.* (1990) indicates an electricity cost increase of only 30%.

For a 500 MW coal-fired plant using air separation/flue gas recycling, the captured flue gas has the following composition after compression and dehydration:

CO_2	122.81 kg/s
H_2O	0
N_2	5.08
O_2	4.02
SO_2	0.86
NO_x	0.23
Total	133.0 kg/s

Table 1.1: Flue gas composition for a 500 MW coal-fired plant using air separation/flue gas recycling [Golomb *et al.* 1989].

We will use these values for the basis of this study to model the release associated with a single 500 MW plant. As CO_2 comprises almost all of this flow, and the behavior of the trace gases will be similar to that of CO_2, we will base our model calculations on a 133 kg/s flow of pure CO_2.

1.2 Scope of this Analysis

Most of these studies have been characterized by only a general examination of the dynamics of an ocean CO_2 release. Calculations from Golomb *et al.* show that with appropriate release conditions, the captured flue gas from a 500 MW power plant

using gas recycling can be completely dissolved in seawater. In this study, we build on the work of Golomb *et al.* in the area of modeling the deep ocean disposal of CO_2. The major differences between the ocean disposal modeling in Golomb, *et al.* and this study are:

a) Golomb *et al.* only considered the liquid CO_2 region below 500 m depth. We consider all depths.

b)Golomb *et al.* just considered individual droplets. We model the entire plume.

The major objective of this research is to understand the dynamic, near-field behavior of CO_2 released in the water column as either a buoyant liquid or vapor. This will involve modeling the behavior of the resulting bubble plume, including bubble rise, mass transfer, possible phase change (depending upon release depth), and potential interaction of bubbles or droplets contained within the plume. This analysis is being conducted using mathematical models that yield the local fate within the water column of CO_2 released as a function of discharge and ambient conditions. The results of this analysis will be used in the conceptual design of a diffuser apparatus to efficiently release the CO_2.

Additionally, we will briefly discuss the ultimate fate of the CO_2 once it has been dissolved in the ocean. Concern at this scale is beyond the dynamic influence of the plume; i.e. hundreds of meters or greater. This transport is more oceanographic in nature and a detailed analysis requires the use of larger scale circulation and transport data and models.

Chapter 2

Model Formulation and Solution

We assume that the CO_2 will be released through one or many ports, each of which may contain an array of smaller orifices. The buoyancy of the CO_2 will induce an upward plume current in the water above each port which will affect the local fate of the CO_2. The near field is being analyzed with two basic models. The simpler bubble or droplet model (which we will refer to as the bubble model for convenience) focuses on the vertical motion and mass transfer associated with a single bubble or droplet, while the plume model solves in addition for the induced water movement created by the continuous release of a collection of buoyant droplets or bubbles from a port. The plume effect increases the absolute velocity of the bubbles or droplets (which equals the water velocity plus the rise velocity relative to the water) and decreases the effective rate of mass transport (due to an increased saturation of the plume water). The two effects combine to increase the height required for CO_2 dissolution. The two basic models have been combined into a single system which simultaneously examines both sets of effects. Conceptually, however, they may be examined separately.

2.1 Physical Properties

2.1.1 Ocean Properties

The vertical profile of the oceans are characterized by an upper mixed layer from the surface to approximately 100 meters below sea level, a thermocline region extending down to about 1000 m, and a deep region extending to the bottom. The upper mixed layer features near-constant density and temperature profiles over the depth, and gaseous concentration levels are in equilibrium with respect to a Henry's Law criteria at the surface. The thermocline region features large gradients of temperature and density over the profile which inhibits vertical mixing. The region below the thermocline is of near-constant temperature, though it is not as well mixed since there are few forces applied to the water. The local, *in situ*, sea water density at these depths increases approximately linearly with pressure as can be seen in Figure 2-1. This figure shows $\sigma_{S,t,p}$ which equals $\rho_{S,t,p}$ - 1000 kg/m^3 where $\rho_{S,t,p}$ is the density of the water with the salinity and the temperature observed and at the pressure appropriate to the observation point. For our buoyancy considerations, we will adopt the practice of adjusting the density with respect to pressure as seen for the same locations in Figure 2-2. This figure shows σ_t which equals $\rho_{S,t,0}$ - 1000 kg/m^3 where $\rho_{S,t,0}$ is the density of the water with the observed temperature and salinity and at atmospheric pressure. This provides an approximate potential density which allows buoyancy comparisons for elevated water.

The exact temperature and density profiles of any particular site vary with the season and with general location. The degree of ambient stratification serves to regulate the maximum rise-height of a release plume, and differences in temperature profiles may change the CO_2 density and solubility at a given depth. To more clearly demonstrate these effects, we have adopted two synthetic profiles based on observations of the Pacific Ocean [McLellan 1965, Stommel *et al.* 1972, Sakai *et al.* 1990, Bialek 1966] as seen in Figures 2-3 and 2-4. These profiles should bracket the likely range of actual conditions, and should show the behavioral sensitivity to varying ocean conditions.

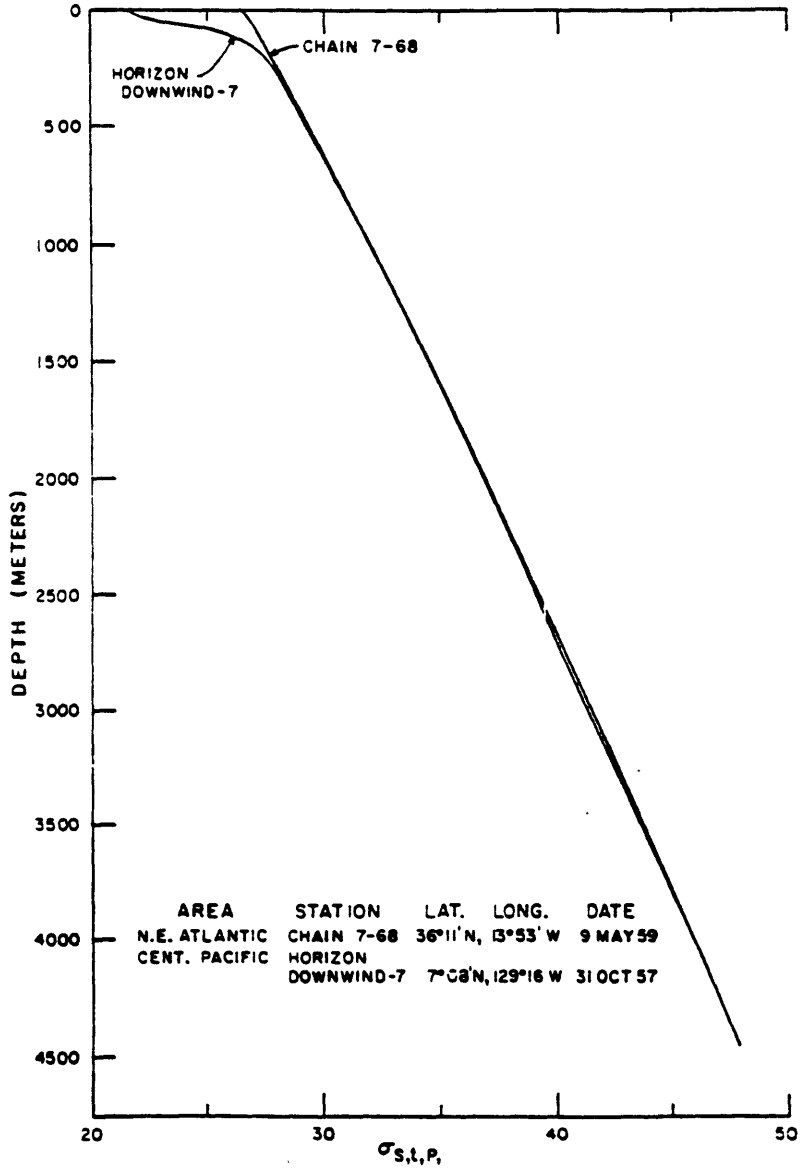

Figure 2-1: $\sigma_{S,t,p}$ vs. depth for two stations. Note $\sigma_{S,t,p} = \rho_{S,t,p}$ - 1000 kg/m^3 where $\rho_{S,t,p}$ is the density of the water with the salinity and the temperature observed and at the pressure appropriate to the observation point [McLellan 1965].

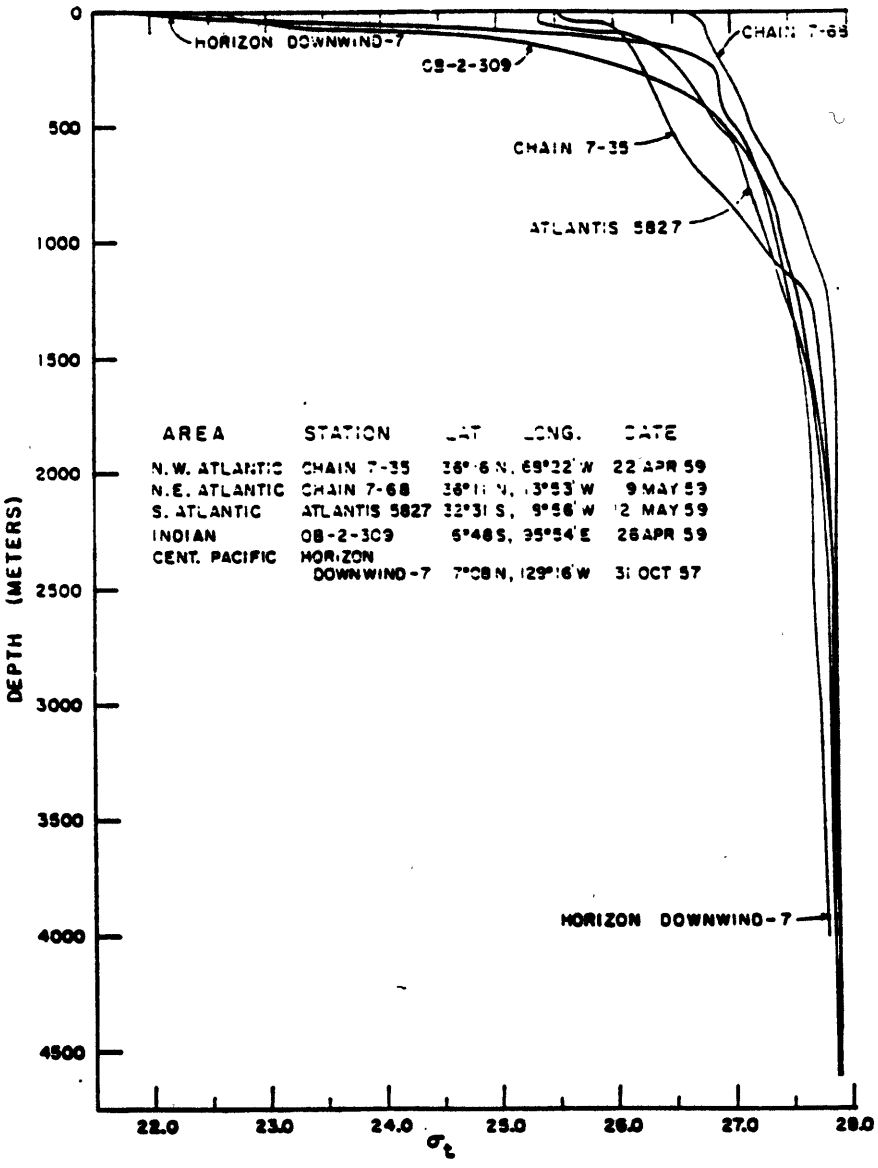

Figure 2-2: σ_t vs. depth at selected stations. Note $\sigma_t = \rho_{S,t,0}$ - 1000 kg/m^3 where $\rho_{S,t,0}$ is the density of the water with the observed temperature and salinity and at atmospheric pressure [McLellan 1965].

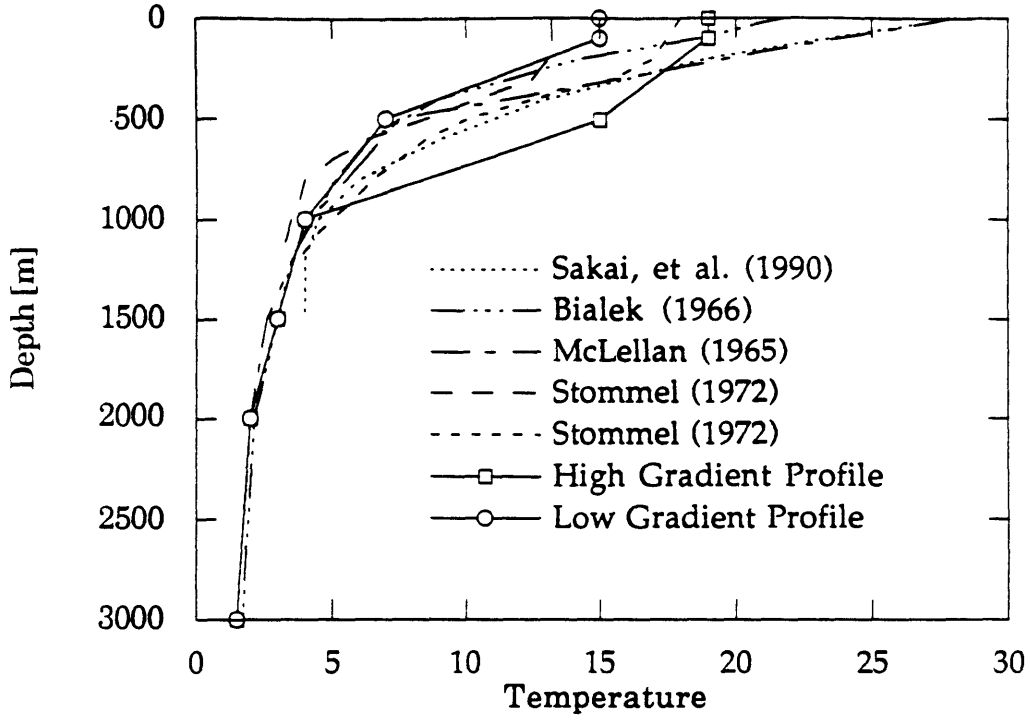

Figure 2-3: Temperature profiles used by model compared to selected literature values.

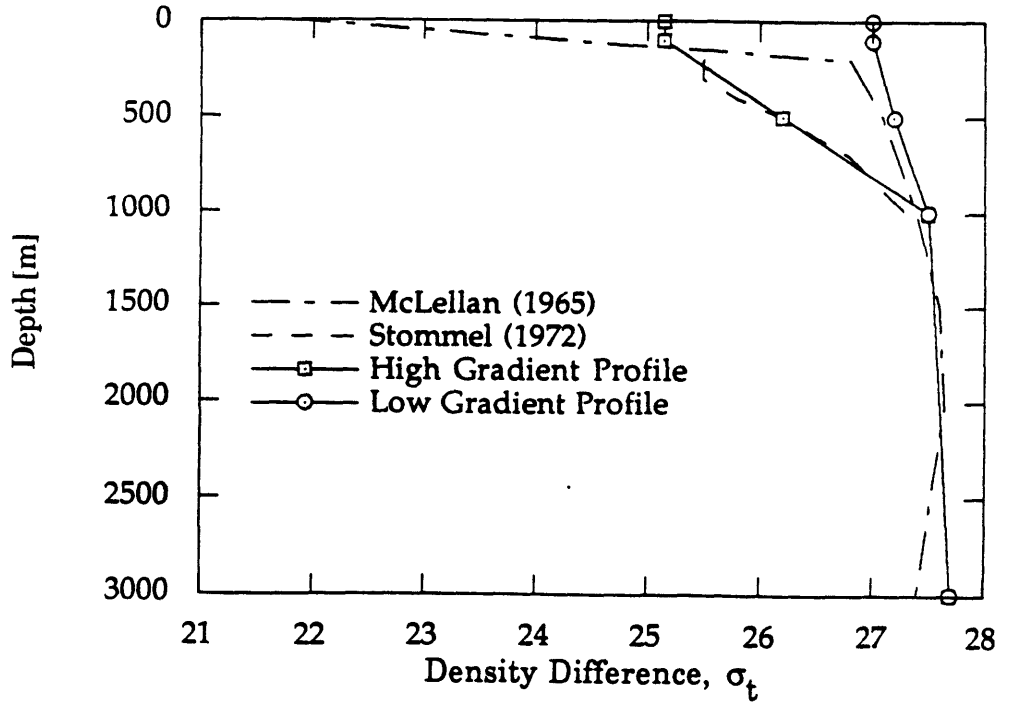

Figure 2-4: Seawater density profiles used by model compared to selected literature values.

2.1.2 CO_2 Properties

Phase and Density

Figure 2-5 shows a phase diagram for CO_2. Given the assumption that the CO_2 temperature and pressure are equal to those of the ambient conditions, this results in liquid CO_2 below a level approximately 500 meters below sea level, and vapor CO_2 above that point. Values for the density of vapor and liquid CO_2 as a function of temperature and pressure may be found in Vargaftik (1975) and Vukalovich (1968). Profiles of CO_2 density versus depth, corresponding to our two synthetic profiles, are shown in Figure 2-6. Note that below roughly 3000 meters, the density of the CO_2 will be greater than that of the seawater, resulting in negative buoyancy below this point.

Furthermore, at depths approximately below 500 meters, the formation of CO_2-hydrates of composition $CO_2 \bullet 6H_2O$ or $CO_2 \bullet 8H_2O$ may occur [Sakai *et al.* 1990, Song and Kobayashi 1987]. This solid precipitate is more dense than the seawater and would tend to sink toward the ocean bottom. The discharge, however, may be complicated by hydrate clogging. Though possibly a significant sink of CO_2, the formation of these hydrates is not well understood. Probably, the amount of hydrate formation will be dependent upon the microdynamic conditions of the interface of the two liquids, which is uncertain at these temperatures and pressures. Thus, hydrate formation will not be taken into consideration in this model. Further analysis of hydrate formation in hydrocarbon plumes has been performed by Topham (1984).

Solubility

The solubility of CO_2 in water is strongly dependent upon the ambient pressure and temperature. Values for solubility have been given by Houghton *et al.* (1957), Wiebe and Gaddy (1940), Stewart and Munjal (1970), and Munjal and Stewart (1971) as a function of temperature and pressure. The salinity of the water, furthermore, will reduce the solubility [Riley and Skirrow 1975, Stewart and Munjal 1970]. Data by Stewart and Munjal (1970) under deep-ocean conditions show a reduction in solubility

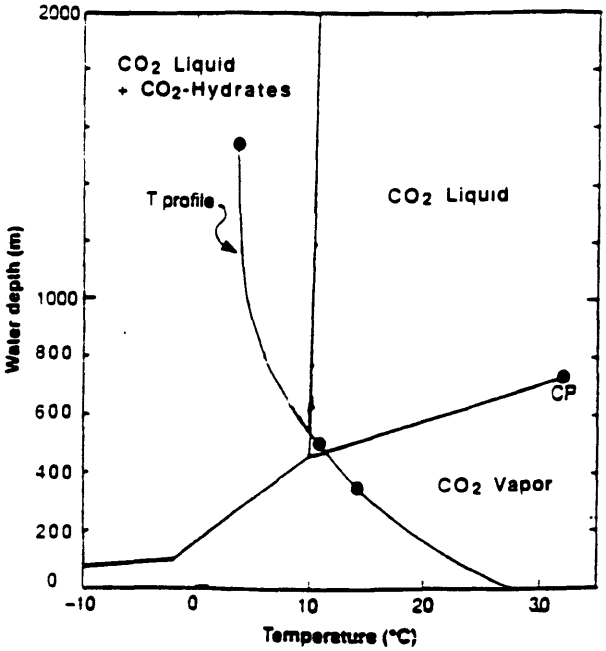

Figure 2-5: Phase diagram for CO_2 for pressures and temperatures associated with the deep ocean. A general temperature profile indicates typical local pressures and temperatures. Adopted from Sakai *et al.* (1990).

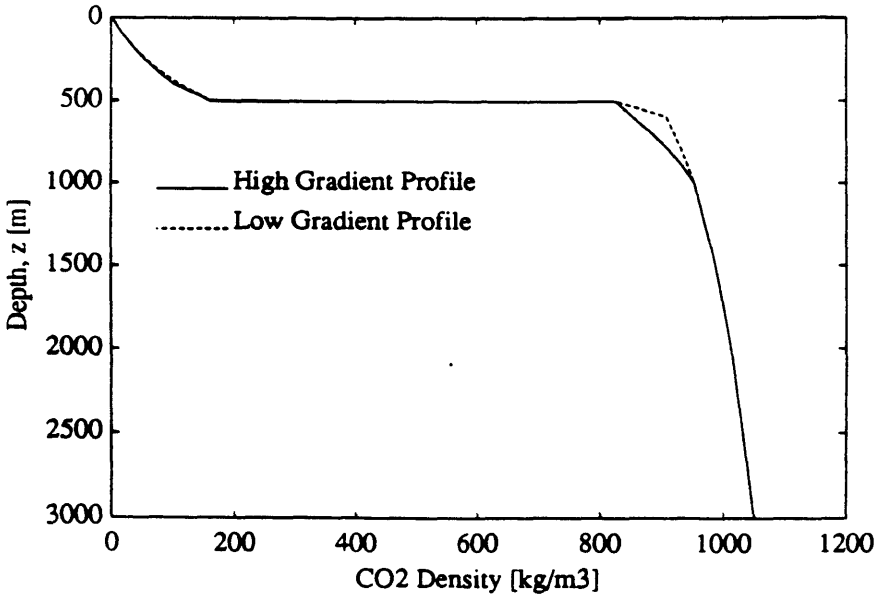

Figure 2-6: CO_2 density profiles used in model.

of about 15% in seawater, therefore we have adopted this modification to the solubility data of pure water. Furthermore, at pressures above 40 atmospheres accompanied by temperatures below 10°C, there is no positive data concerning CO_2 solubility in water, and the above researchers have noted difficulty because of the formation of hydrates and because of the liquid CO_2 becoming miscible with the water. These possibilities may significantly affect the fate of CO_2 released at these depths, but as there remains uncertainty we will adopt a conservative model assuming immiscible bubbles and a solubility of 51 kg/m^3. Our modeled values for solubility at depth z may be seen in Figure 2-7 which shows the impacts of temperature variation between our two profiles.

Ambient CO_2 concentrations are shown in Figure 2-8 [Riley and Skirrow 1975] for a Pacific Ocean location. The maximum observed concentration of $2.4 \cdot 10^{-3}$ moles/kg is equivalent to 0.108 kg CO_2/m^3 of seawater, and the entire range is approximately 0.1 kg/m^3, which is much less than the solubility level.

2.2 Bubble Model

The bubble model examines the mass transfer and terminal rise velocity associated with a single bubble or droplet of CO_2. For our analysis, these may be CO_2 vapor bubbles or CO_2 liquid droplets. The model assumes that the temperature and pressure of each bubble are equal to the ambient temperature and pressure. This implies that heat transfer is assumed to be instantaneous, and that the pressure contribution from surface tension is negligible. Furthermore, we assume that the properties are homogeneous within each bubble, and that the phase change from liquid to vapor occurs instantaneously at 500 meters.

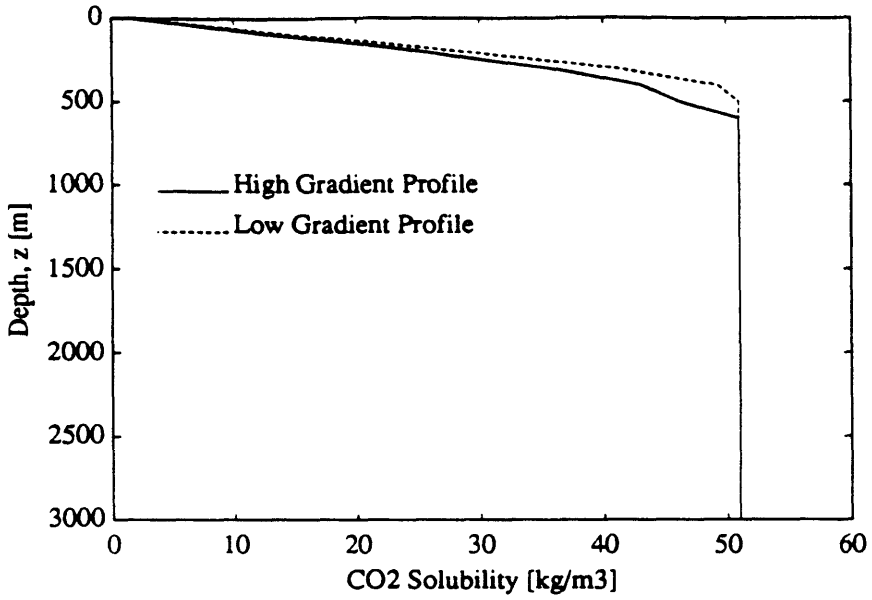

Figure 2-7: CO_2 solubility profiles used in model.

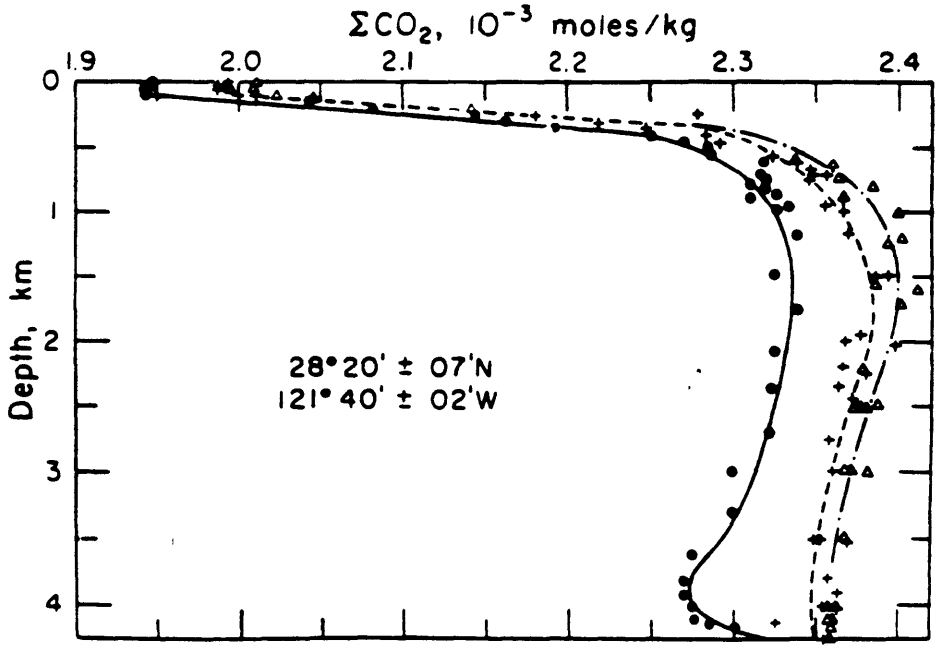

Figure 2-8: Ambient CO_2 levels [Riley and Skirrow 1975].

2.2.1 Physical Structure

Release Size

As CO_2 is released into the ocean, different physical characteristics of the bubbles will occur as a function of the rate of release and the diameter of the release orifice. Bubble or droplet formation at an orifice can be said to occur within one of three different regimes [Clift *et al.* 1978]. For slow flows, individual bubbles will form at the orifice. In this case, the surface tension of the bubble provides the major restraining force against separation, and thus the size of the orifice plays an important role. At larger flows, a jet protrudes from the orifice, and bubbles are formed by jet breakup. At still higher flows, the injected fluid shatters at or very near the orifice to give many droplets by a process of atomization. For the rather large magnitude of the modeled flows, about 1 m^3/s, the release will be as a jet or will be atomized depending upon the exact characteristics of the diffuser apparatus. Most experimental investigations of bubble plumes have involved releases much les s than 1 m^3/s which would most likely fall into the first or second category. The exact performance of any particular diffuser apparatus, particularly one which shatters the release, however has not been thoroughly investigated at these large flows. Our modeling will assume that the release diameter of a CO_2 bubble or droplet is variable given design considerations of the diffuser. The maximum or minimum size at any given high flow rate, however, are uncertain.

Maximum Size Due to Dynamic Instability

Another aspect of bubble size is associated with the dynamic stability of the surface of a bubble or droplet. An expression for this maximum effective droplet radius is given by Clift *et al.* (1978) and by Hu and Kinter (1955).

$$r_{max} \simeq 1.9\sqrt{\frac{T}{g(\rho_w - \rho)}} \tag{2.1}$$

where T is the interfacial surface tension between water and the CO_2, g is gravitational acceleration, ρ_w is the water density, and ρ is the droplet density. Applying this relationship to CO_2 liquid droplets, we find that the maximum radius is approximately 1.25 cm. While this equation is not appropriate for determining the maximum vapor bubble sizes, Clift *et al.* (1978) cites a maximum air bubble radius of about 2.5 cm. These values, then, allow us to consider the maximum possible size of a bubble at the plume origin. Moreover, these values do not take into account the fragmentation induced by the plume turbulence, nor the effects of water contaminants which will decrease the strength of a bubble or droplet and result in smaller sizes. The actual maximum bubble size, therefore, will likely be somewhat less.

Large Bubble Shape

At diameters above about 1.0 mm, the bubbles or droplets are not actually spherical, but may be characterized as ellipsoidal or spherical-cap depending upon the size. For analysis of these non-spherical bubbles, an equivalent diameter, defined as the diameter of a sphere of equal volume, is used. Ellipsoidal bubbles usually occur for effective diameters between 1 and 15 mm. These bubbles tend to rise not in straight lines, but in a helical or zig-zag path [Clift *et al.* 1978]. Larger bubbles or droplets approximate spherical caps, with a rounded front and a flat base. Most of the CO_2 with the release plume will be in the form of these spherical-cap bubbles or droplets.

Coalescence

This model assumes that individual bubbles are isolated enough so that they do not significantly coalesce with surrounding bubbles. Such a consideration facilitates the modeling of mass transfer, and in the limit of a decreasing bubble size it is apparent that any coalescence would decrease as the bubbles became smaller and spread further out. McDougall (1978), however, sites photographic evidence by Jones (1972) in making the assumption that within a bubble plume the bubble size remains constant due to a balancing of coalescence and dynamic fragmentation. He proposed that the bubble size within the plume was dependent only upon the intensity of the turbulence.

This evidence, however, was derived from plumes of a much smaller scale in which a high concentration of bubbles led to increased coalescence and fragmentation, and in which mass transfer was not a factor. The exact relationship between coalescence and turbulent fragmentation in a plume of this magnitude, however, is uncertain and may significantly impact the effectiveness of a release structure dependent upon small bubble size.

2.2.2 Bubble Dynamics

A conservation of mass equation, based on a mass transfer expression, that governs the rate of dissolution of a spherical bubble is given by

$$\frac{d}{dt}\left[\frac{4}{3}\pi r^3 \rho\right] = -4\pi r^2 K\left[\mathrm{C}_s - \mathrm{C}_\infty\right] \tag{2.2}$$

where K [length/time] is a mass transfer coefficient, ρ is CO_2 density, C_s is the surface concentration of dissolved CO_2, which is assumed to be at saturation, and C_∞ is the far-stream, ambient concentration of dissolved CO_2. This equation can be simplified to calculate the change in radius r of a gas bubble as a function of elevation z.

$$-\frac{dr}{dt} = \frac{K\left(\mathrm{C}_s - \mathrm{C}_\infty\right)}{\rho} - \frac{r\frac{d\rho}{dz}(U_b + U)}{3\rho} \tag{2.3}$$

or

$$\frac{dr}{dz} = \frac{K\left(\mathrm{C}_s - \mathrm{C}_\infty\right)}{\rho(U_b + U)} - \frac{r\frac{d\rho}{dz}}{3\rho} \tag{2.4}$$

where U_b is the terminal bubble rise velocity and U is the velocity of the surrounding water. For modeling purposes, we will focus on the fastest moving bubbles such that the plume velocity used for bubble transport is equivalent to the centerline velocity of the plume. In a pure single bubble model, $U = 0$. The first term on the right hand side of Equations (2.3) and (2.4) is the mass-transfer term, while the second is a compressibility term. Furthermore, if $\mathrm{C}_s \gg \mathrm{C}_\infty$, we may make the approximation that $\mathrm{C}_s - \mathrm{C}_\infty \simeq \mathrm{C}_s$.

The major independent parameters of this equation are the gas transfer rate K

and the slip velocity U_b. We examine the values of these parameters appearing in a number of previous investigations.

Many previous models of bubble plumes [Milgram 1983, Cederwall and Ditmars 1970, McDougall 1978] have made the approximation that the slip velocity of an individual bubble is constant, ranging from 28 to 35 cm/s. These same studies also did not include mass transfer, and so K was not addressed. Rayyan (1972) did allow for variable slip velocity, though his functions were not applicable for larger bubble sizes.

Specific research on bubble and droplet dynamics, however, has focused on rise velocities and mass transfer coefficients associated with these large bubbles. Because of the non-spherical shape and the mobile surface of a bubble, the commonly applied Stokes' terminal velocity law which balances buoyancy with the drag resistance associated with a rigid particle, is not applicable with much accuracy. Rather, investigations have been empirical in nature, resulting in formulas associating U_b and K with the effective radius of the bubble, the slip velocity, and the density difference with the surrounding fluid.

Mass Transfer Formulas

Clift *et al.* (1978) separated the formulas along the three basic bubble structure regimes. A general expression for K for spherical-cap bubbles or droplets is given as

$$K = 1.25 \left(g \frac{\rho_w - \rho}{\rho_w} \right)^{1/4} \mathcal{D}^{1/2} d^{-1/4} \tag{2.5}$$

where $\mathcal{D}$ = molecular diffusivity, and d = the effective diameter. An expression for smaller bubbles is given as

$$K = \frac{2}{\sqrt{\pi}} \left(\frac{U_b \mathcal{D}}{d} \right)^{1/2} \tag{2.6}$$

Regarding K, Weiner and Churchill (1977) and Weiner (1974) cite Boussinesq (1905) and secondary references for a boundary layer expression for a mobile surface

$$\mathrm{Sh} = 1.128 \left(\Re \, \mathrm{Sc} \right)^{1/2} \tag{2.7}$$

where Sh is a Sherwood number defined as $(2rK/\mathcal{D})$, $\Re$ is the bubble Reynolds number defined as $(2rU_b/\nu)$, and Sc is a molecular Schmidt number defined as $(\nu/\mathcal{D})$ where $\mathcal{D}$ = molecular diffusivity and ν = viscosity of ambient fluid. This relationship is identical to that found in Equation (2.6).

Alternatively, Cussler (1984) suggests the relationship for drops or bubbles in a liquid solvent as

$$\mathrm{Sh} = 0.42 \left[\frac{8r^3(\rho_w - \rho)g}{\rho_w \nu^2}\right]^{1/3} \left[\frac{\nu}{\mathcal{D}}\right]^{1/2} \tag{2.8}$$

This relationship gives K as a function of ρ which varies with depth, but does not demonstrate as much variability as functions dependent on bubble size.

As seen in Figure 2-9, Equation (2.8) tends to give larger values than the other references. This Figure is based on an initial radius of 2.0 cm released at 500 m to allow for a single independent variable for these expressions. Furthermore, Equation (2.5) for spherical-cap bubbles gives somewhat larger values than Equations (2.6), or (2.7). We have adopted Equation (2.5) as it takes into account the particular dynamics of a large bubble. We will demonstrate the sensitivity to this coefficient in the discussion of model sensitivity.

Slip Velocity Formulas

Clift approached slip velocities also through focusing on each level of bubble size. An expression for spherical-cap bubbles or droplets is given as

$$U_b = 0.711\sqrt{g\,d\,\frac{\rho_w - \rho}{\rho_w}} \tag{2.9}$$

and for ellipsoidal bubbles

$$U_b = \left[\frac{2.14\,\mathrm{T}}{\rho_w\,d} + 0.505\,g\,d\right]^{1/2} \tag{2.10}$$

Alternatively, a relationship for U_b, established by Aybers and Tapucu (1969), is

cited by Weiner and Churchill (1977)

$$U_b = \left[\frac{4\,g\,\nu}{3}\right]^{1/3}\left[\frac{108.4}{Z} + \sqrt{\frac{Z}{0.5479}}\right] \tag{2.11}$$

where $Z = 0.434r(g/\nu^2)^{1/3}$. Figure 2-10 shows profiles of bubble slip velocities given a release of 2.5 cm radius bubbles from 500 m, and indicates that these expressions give generally similar results. We have adopted Equation (2.11) as our expression for bubble velocities.

It can be expected that the slip velocities associated with liquid droplets will not be as large due to the much lower buoyancy per unit mass. Clift's expression for spherical-cap bubbles, Equation (2.9) may be solved for liquid droplets as well as bubbles. Alternatively, Treyball (1963), in a discussion of liquid droplets, gives an expression cited in Golomb such that

$$U_b = \frac{17.6\,(\rho_w - \rho)^{.28}\,\nu^{.10}\,\mathrm{T}^{.18}}{\rho^{.45}} \tag{2.12}$$

Note that this expression gives U_b independent of r.

Equation (2.12) tends to give faster values as seen in Figure 2-11. We have adopted Clift's Equation (2.9) as it gives somewhat more conservative results and it is specifically oriented toward larger bubbles. We will also examine the sensitivity of rise velocity, furthermore, in the discussion of model sensitivity.

As a droplet or bubble becomes very small, the slip velocity will approach zero. The above velocity expressions are for large bubbles and are not valid for $r \lesssim 0.3$ cm. Because almost all of the CO_2 has gone into solution by the time this size is reached, we will apply the formulas for larger bubbles throughout the plume. These formulas will give slip velocities which are larger, resulting in a droplet traveling further before dissolving; as such, the formulas are conservative.

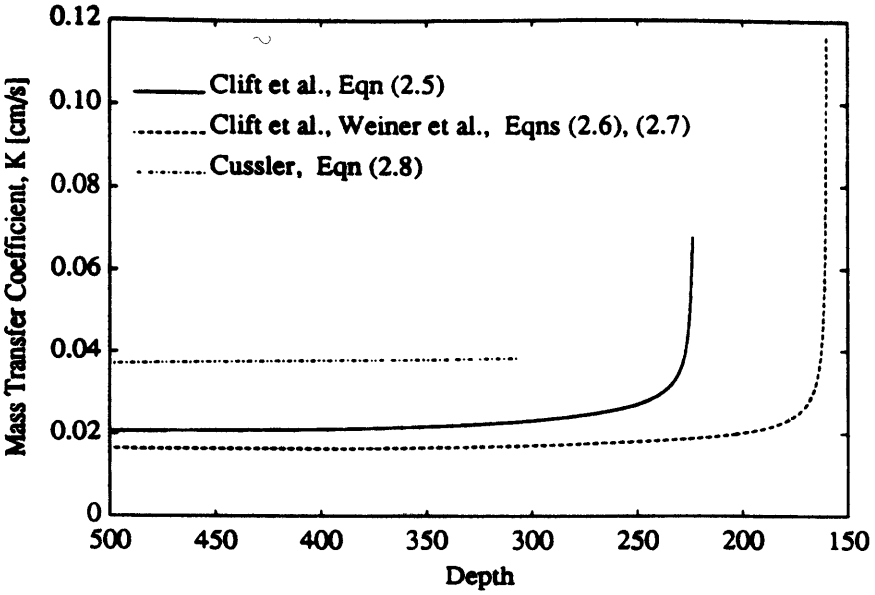

Figure 2-9: Comparison of mass transfer coefficient formulas for a 2 cm radius bubble released at 500 m.

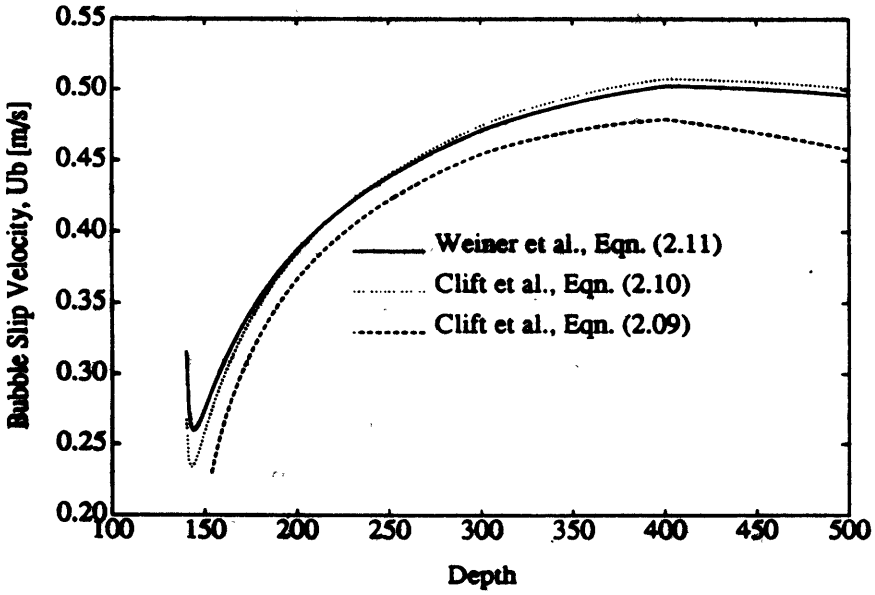

Figure 2-10: Comparison of bubble slip velocity predictions for 2.5 cm radius bubbles released at 500 m.

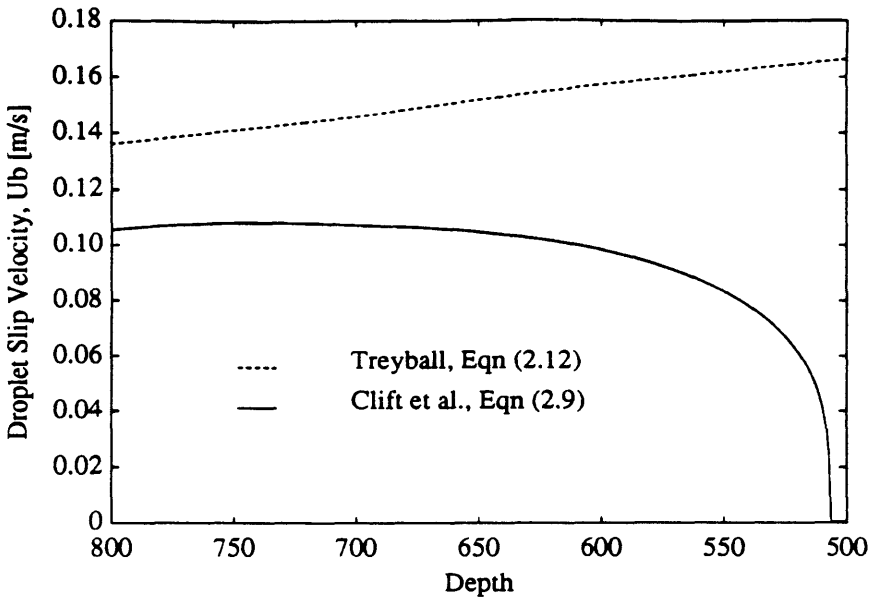

Figure 2-11: Comparison of droplet slip velocity predictions.

2.3 Plume Model

2.3.1 Background

The subject of buoyant plumes has been studied extensively, and the similarity between an air-bubble plume and a simple buoyant plume was first pointed out by Taylor (1955) in a study of pneumatic breakwaters. Bulson (1968) also examined bubble breakwaters, primarily focusing on the surface flows rather than the plume structure. Kobus (1968) performed experimental measurements of internal bubble plume velocities, and developed a simple mathematical model based on momentum conservation. Jones (1972) performed principally experimental work focusing on the surface interaction with an oil slick. Cederwall and Ditmars (1970) and Milgram (1983) developed integral models for an unstratified ambient based on mass and momentum conservation and using an entrainment law. Rayyan (1974) and Speece (1973) used a model similar to Cederwall and Ditmars, and included the effects of mass transfer and a stratified ambient in an investigation of lake aeration, but did not develop a model of the separation of the bubbles past the point where a sim-

ple plume would stall. McDougall (1978) did examine this issue and developed a double-plume model in which a central conical bubble-filled plume was nested within an annular plume containing only liquid. This model, however, did not include the effects of mass transfer, and thus did not allow for the disintegration of the bubbles. Hussain and Narang (1984), developed a model similar to McDougall (1978) which incorporated stratification effects, but which used an energy conservation law to develop the plume equations. Chesters *et al.* (1980) developed a general model with a particular emphasis on non-dimensional parameters and turbulent momentum. McDougall (1981) further developed the double-plume model with an emphasis on the top of a normally-buoyant plume in a stratified ambient. Leitch and Baines (1989) examined the dynamics particular to small-scale bubble plumes. Tsang (1984) examined the dynamic similarity between prototype and model bubble plumes. Sun and Faeth (1986) examined the turbulent structure of bubbly jets. Goossens and Smith (1975) and Godon and Milgram (1987) examined principally the vertical mixing associated with a bubble plume in connection with lake and reservoir destratification. Baddour (1990) examined vertical heat transport using bubble plumes as a means of ice prevention.

2.3.2 Plume Dynamics

A bubble plume is different from a plume driven by a normal source of buoyancy in four important respects. First, the buoyant forces are dependent on the volume flow rate of the bubbles, which tends to increase with height as the pressure decreases and which may decrease with height due to mass transfer from the bubbles into the surrounding liquid. Second, the bubbles will rise faster than the liquid surrounding them. Third, the driving buoyancy, provided by the bubbles, is more concentrated toward the center of the plume. Fourth, in a stratified environment, the bubbles will usually continue to rise past any height at which simple plume theory predicts that the plume would stop rising and spread horizontally. For an ordinary plume in a stratified environment, a height is reached at which the buoyancy is zero. As inertia carries the plume above this level, it continues to slow down while gaining negative

buoyancy. Eventually, it stops rising and settles horizontally at a level somewhat less than the maximum height.

Our model uses the horizontally integrated equations of conservation of mass, momentum, and buoyancy as presented in Morton, Taylor, and Turner (1956) and makes the Boussinesq approximation for buoyant flows that density differences within the water are very small compared to the difference with the CO_2 and that the density of the water is much greater than the CO_2 density. Furthermore, the plume model adopts a mean-flow theory based on the assumption that lateral profiles of plume properties (velocity, water density deficiency, and dissolved and gaseous CO_2 concentration) are similar at all heights and that they can be approximated by Gaussian distributions, as adopted in Kobus (1968) Cederwall and Ditmars (1970), Rayyan (1974), and Milgram (1983).

Thus a velocity profile is given

$$U = U_m \, e^{-R^2/b^2} \tag{2.13}$$

where U is a local mean velocity, U_m the centerline, maximum velocity, R is the radial distance from the centerline, and b is the nominal half width of the plume related to the standard deviation of the velocity distribution, σ, by $b = \sqrt{2}\sigma$ as shown in Figure 2-12.

Similarly

$$C = C_m \, e^{-R^2/(\lambda_1 b)^2} \tag{2.14}$$

and

$$\rho_w - \rho_a = \Delta\rho_{w,m} \, e^{-R^2/(\lambda_2 b)^2} \tag{2.15}$$

where C = concentration of volume of gas per unit plume volume, ρ_w is the water plume density, ρ_a is the ambient water density at any level, $1/\lambda^2$ is a turbulent Schmidt number, and the subscript m denotes a center line (maximum) value. The term $\lambda_1 b$ can be construed as the nominal width of the gas-carrying portion of the

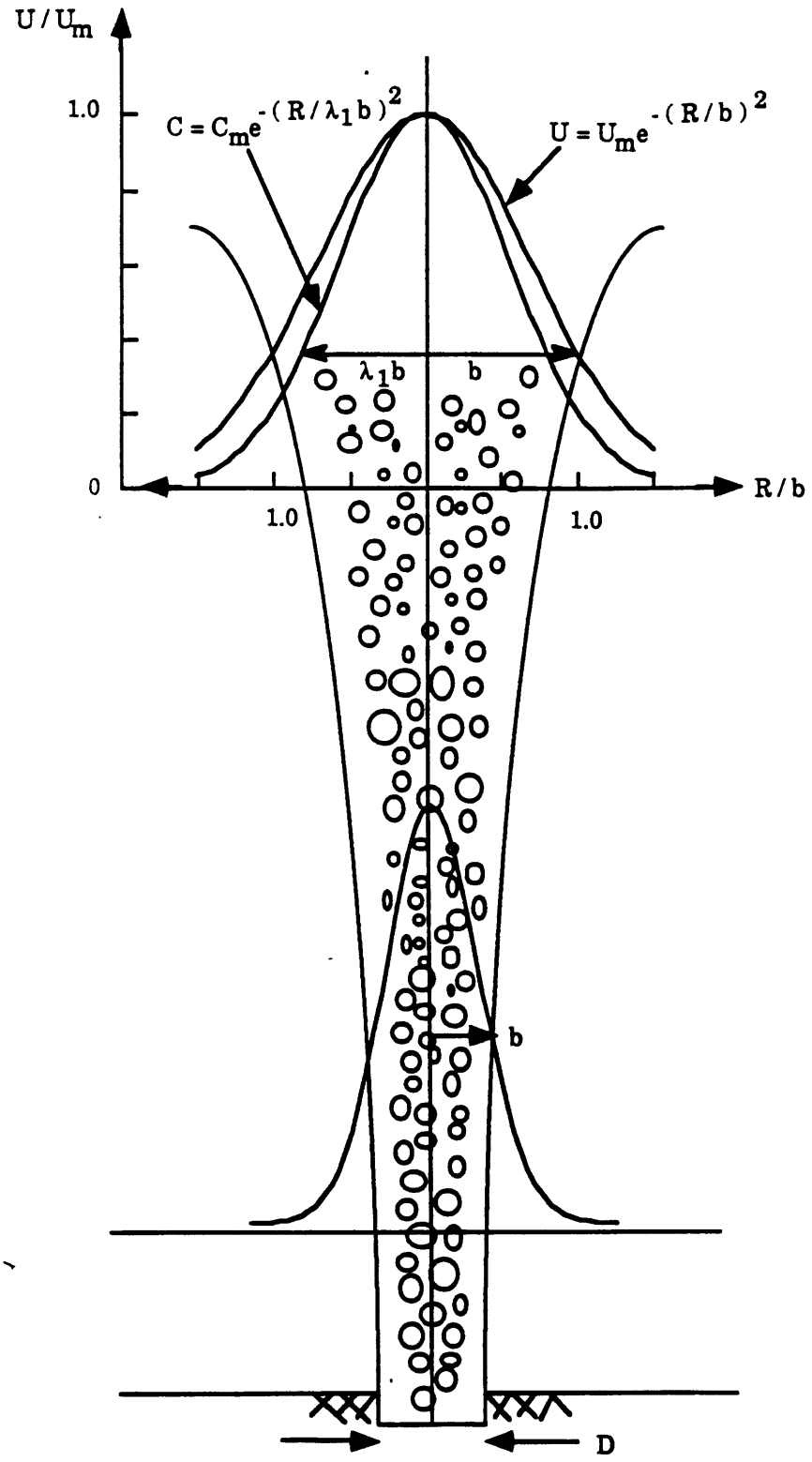

Figure 2-12: Schematic of a bubble plume.

plume, and λ_1 and λ_2 can be seen as a spreading ratio with respect to velocity. A mixture density expression may also be written

$$\rho_{\text{mix}} = C\,\rho + (1 - C)\,\rho_w \tag{2.16}$$

The expression for the liquid volume flux is written

$$\mathrm{Q} = \int_0^\infty (1 - C) 2\pi U R\, dR \simeq \pi U_m b^2 \tag{2.17}$$

where we assume $C \ll 1$.

The rate of entrainment of ambient water into the water plume is established with the assumption that the entrainment velocity, U_e, is proportional to the centerline velocity such that $U_e = \alpha U_m$, where α is defined as an entrainment coefficient. Thus conservation of liquid volume implies

$$\frac{d\mathrm{Q}}{dx} = 2\pi\alpha b U_m \tag{2.18}$$

or

$$\frac{d}{dx}\left[U_m b^2\right] = 2\alpha b U_m \tag{2.19}$$

where x is taken as the upward distance from the plume origin. Note that x is used to designate upward distance from the release, while z corresponds to a particular depth below the surface.

The volumetric gas flow is a function of pressure, and thus height, and is also dependent upon the amount of CO_2 which has gone into solution. Using the bubble model to calculate a bubble radius at a given depth, r_z, conservation of CO_2 mass leads to a CO_2 volume flux

$$\mathrm{q}_z = \mathrm{q}_{\text{rel}} \left(\frac{r_z}{r_{\text{rel}}}\right)^3 \tag{2.20}$$

where q_z is the gas volume flow rate at depth z, r_{rel} is the bubble radius at release depth (500 m for phase change considerations), and q_{rel} is the volume flow at the

release point. Other bubble plume models have assumed that q_z increased linearly with pressure. We have allowed for mass transfer and a non-linear CO_2 density profile in our evaluation of q_z.

Carbon-dioxide volume flux may also be expressed in terms of volumetric plume concentration such that

$$q_z = \int_0^\infty 2\pi C(U + U_b) R\, dR = U_m C_m \pi \frac{b^2 \lambda_1^2}{1 + \lambda_1^2} + U_b C_m \pi b^2 \lambda_1^2 \tag{2.21}$$

This equation may be used to solve for C_m such that

$$C_m = \frac{\frac{q_z}{\pi b^2 \lambda_1^2}}{\left[U_m \frac{1}{1+\lambda_1^2} + U_b\right]} \tag{2.22}$$

The buoyancy, B, of the plume is derived from the positive buoyancy of the carbon dioxide and from any liquid density difference caused by stratification.

$$B_z = \int_0^\infty 2\pi g(\rho_a - \rho_{\text{mix}}) R\, dR \tag{2.23}$$

where ρ_a is the local density of the ambient water.

Furthermore, the plume momentum, M, may be defined

$$M = \gamma \int_0^\infty 2\pi U^2 \rho_{\text{mix}}\, R\, dR \tag{2.24}$$

where γ is a momentum amplification factor introduced by Milgram (1983) to incorporate the portion of the mean momentum flux carried in the turbulence and is defined as the ratio of the total momentum flux to the momentum flux of the mean flow.

Finally, as buoyancy is assumed to be the only force acting upon the plume, it may be related to the momentum such that

$$\frac{dM}{dx} = B_z \tag{2.25}$$

The assumption of profile similarity for a bubble plume implies that plume property profiles cannot evolve with distance, and thus the buoyancy, B, is similarly distributed over the plume cross-section at any x. The total buoyancy of a bubble plume in a stratified environment is composed of independent positive and negative components. If the relative magnitudes of the two terms remain constant, similarity could be achieved. As this is not usually the case due to density gradient effects in addition to the changing bubble size, similarity may still be achieved if both are similarly distributed, i.e. $\lambda_1 = \lambda_2$. Experimentation shows, moreover, that in fact these are not equal for bubble plumes. The assumption of self-similarity, therefore, is violated as $\Delta\rho_{w,m}$ grows in magnitude. This violation may be associated with the uncoupling events which have been observed in bubble plumes.

It follows from Equations (2.23), (2.24), and (2.25) that

$$\frac{d}{dx}\int_0^\infty 2\pi\gamma U^2 \rho_{\text{mix}} R\, dR = \int_0^\infty 2\pi g(\rho_a - \rho_{\text{mix}})\, R\, dR$$

Making the Boussinesq assumption for buoyant flows, assuming that γ is constant, and adopting a reference water density ρ_{ref}, taken at the release depth, this may be simplified

$$\frac{d}{dx}\left[\frac{1}{2}\pi\gamma b^2 U_m^2\right]\rho_{\text{ref}} = g\pi b^2\lambda_1^2 C_m\,(\rho_w - \rho) - g\pi b^2\lambda_2^2\Delta\rho_{w,m}$$

or

$$\frac{d}{dx}\left[b^2 U_m^2\right] = \frac{2gb^2}{\gamma}\left[\lambda_1^2 C_m\frac{\rho_{\text{ref}} - \rho}{\rho_{\text{ref}}} - \frac{\lambda_2^2\,\Delta\rho_{w,m}}{\rho_{\text{ref}}}\right] \tag{2.26}$$

Furthermore, the effects of ambient stratification are included by separately examining the portion of the buoyancy resulting from differences in water density, B_w, as demonstrated in Rayyan (1974). Let

$$B_w = \int_0^\infty 2\pi\,(\rho_{\text{ref}} - \rho_w)\, R\, dR$$

Assuming a linear relationship between temperature and density, conservation of thermal energy may be represented as buoyancy conservation. Incorporating the

entrainment model, conservation of buoyancy flux gives

$$\frac{d}{dx}\int_0^\infty 2\pi U\left(\rho_{\text{ref}}-\rho_w\right) R\, dR = 2\pi b\alpha U_m\left(\rho_{\text{ref}}-\rho_a\right)$$

which reduces to

$$\frac{d}{dx}\left[U_m b^2\left(\left(\rho_{\text{ref}}-\rho_a\right)-\frac{\lambda_2^2\,\Delta\rho_{w,m}}{1+\lambda_2^2}\right)\right] = 2b\alpha U_m\left(\rho_{\text{ref}}-\rho_a\right)$$

and substituting Equation (2.19), this may be simplified to

$$\frac{d}{dx}\Delta\rho_{w,m} = -\frac{1+\lambda_2^2}{\lambda_2^2}\frac{d\rho_a}{dx}-\frac{2\alpha\Delta\rho_{w,m}}{b} \tag{2.27}$$

where $\frac{d\rho_a}{dx}$ is the local ambient density gradient.

Finally, Equations (2.19), (2.26), and (2.27) may be expressed in terms of the three unknowns b, U_m, and $\Delta\rho_{w,m}$ as differential equations with respect to depth z.

$$\frac{db}{dz} = -2\alpha+\frac{gb}{\gamma U_m^2}\left[C_m\lambda_1^2\frac{\rho_{\text{ref}}-\rho_g}{\rho_{\text{ref}}}-\frac{\Delta\rho_{w,m}\,\lambda_2^2}{\rho_a}\right] \tag{2.28}$$

$$\frac{dU_m}{dz} = -2\frac{g}{\gamma U_m}\left[C_m\lambda_1^2\frac{\rho_{\text{ref}}-\rho_g}{\rho_{\text{ref}}}-\frac{\Delta\rho_{w,m}\,\lambda_2^2}{\rho_a}\right]+\frac{2\alpha U_m}{b} \tag{2.29}$$

$$\frac{d\Delta\rho_{w,m}}{dz} = -\frac{1+\lambda_2^2}{\lambda_2^2}\frac{d\rho_a}{dz}+\frac{2\alpha\,\Delta\rho_{w,m}}{b} \tag{2.30}$$

With C_m substituted from Equation (2.22), the characteristics of the plume may be solved from these equations.

2.3.3 Plume Parameters

This model relies on four parameters: the entrainment coefficient α, the gas concentration spreading ratio λ_1, the water density spreading ratio λ_2, and the momentum amplification factor γ. The values for these coefficients were taken from experimental analysis performed by previous investigators.

Cederwall and Ditmars (1970) adopted a constant value for α based on the data of Kobus (1968) for the case of a point source bubble plume which indicated a growth in α with the air flow rate reaching asymptotically a value of about 0.08. Similarly, Rouse *et al.* (1952) found a value of $\alpha = 0.082$ for the case of a three-dimensional simple plume. Milgram (1983) adopted a theory that the entrainment coefficient was not constant, but rather depended upon the degree of turbulence within the plume, as characterized by a bubble Froude number. This analysis showed values of α from 0.04 to 0.14. Rayyan (1974) attempted to express α as a function of the density gradient of the ambient atmosphere, but found little correlation and so adopted a constant value of 0.04 calibrated against laboratory data and 0.055 calibrated against larger-scale experiments performed in a lake.

A broad range of values of λ_1 have been reported in previous studies. Cederwall and Ditmars (1970) state that the lateral rate of spreading of the air-bubbles is slow relative to the expansion of the plume, and cite photographic data indicating a fairly constant value of 0.2. Fannelop and Sjoen (1980) used a value of 0.6, also based on photographic observations. Milgram and Van Houten (1982) used a comparison of measured radial profiles of velocity and gas fraction which resulted in an average value of 0.8. Rayyan (1974) cited Cederwall and Ditmars (1970) and chose a constant value of 0.2. This wide range may be due to differences associated with the bubble size. As bubbles become infinitely small, they will be transported with zero slip such that λ_1 may be seen to approach λ_2, i.e. values comparable with or greater than one. As the bubbles increase in size, however, the upward slip velocity will increase causing a higher concentration in the center and thus lower values o f λ_1.

The use of λ_2 in a bubble plume model is limited to the work by Rayyan involving a stratified atmosphere. This experimental data gave a value of $\lambda_2 = 1.25$. This parameter, however, is representative of temperature spreading and thus is similar to values for spreading ratios of thermal plumes, which are cited to be about 1.1 [Rouse *et al.* 1952]

Milgram (1983) extensively discusses the momentum amplification factor, γ. High values of γ are associated with large turbulent velocities compared with the mean.

Using relationships based on plume and bubble length-scales, velocity, and density, it was found that high values of γ occur in plumes characterized by a relatively slow mean flow and relatively widely spaced bubbles. For this case, much of the momentum is carried by the distinct wakes of the bubbles. For larger, more concentrated plumes, however, the wakes of the bubbles are merged together so that the turbulent velocities are relatively small in comparison to the mean. For a plume of our prototype scale, therefore, the value of γ is approximately equal to unity.

For our model predictions, we have adopted a set of constant parameters such that $\alpha = 0.1$, $\lambda_1 = 0.8$, $\lambda_2 = 1.25$, and $\gamma = 1.0$. The potential variability of these parameters, particularly α, affects the impact of the plume on the CO_2 fate. Appendix A details a model sensitivity analysis of these parameters.

2.3.4 Bubble Plume Peeling/Uncoupling

The eventual fate of the CO_2 enriched water is ultimately dependent upon the effects of the ambient density gradient. If a stream of soluble bubbles is released into an atmosphere of constant density, the bubble plume will reach a height where all the bubbles have dissolved. The plume at this point, however, has a certain amount of upward momentum, which will remain constant over the height of the water column. This jet behavior will serve to transport the enriched water contained within the plume structure to the surface, thus releasing the dissolved gas into the atmosphere. The presence of an ambient density gradient, however, will counteract this action. As denser water is entrained from deeper depths and carried up into a less-dense ambient atmosphere, a negatively buoyant force will exist which opposes the positive buoyancy of the bubbles. In plumes driven by a normal source of buoyancy, this stratification will result in the plume reaching a maximum height. In a bubble plume, however, this theoretical maximum height, i.e. where the negative buoyancy has caused the plume to decelerate to zero velocity, may be reached while bubbles are still present in the plume. Because the bubbles are still locally strongly positively buoyant, an uncoupling or peeling of the dense water from the bubbles must occur. This effect has been noted by Cederwall and Ditmars (1970) and Rayyan (1974). McDougall

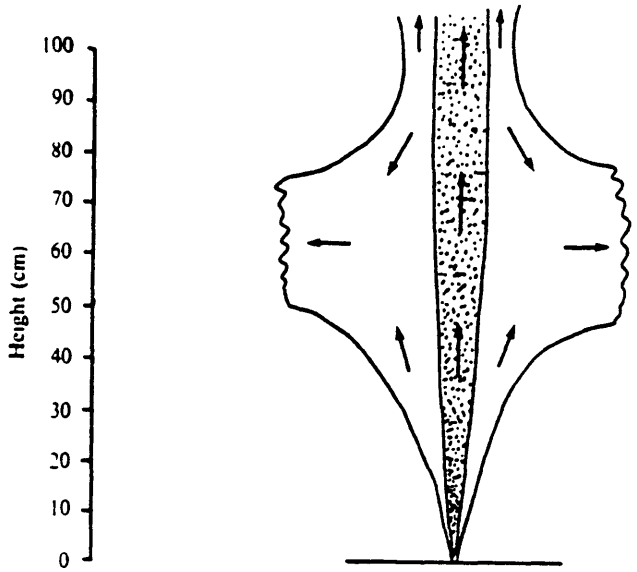

Figure 2-13: Diagram of McDougall (1978) experiment.

(1978) attempted to model this effect using his double-plume model. Figure 2-13 [McDougall 1978] shows an example of his experimental results. In this example, a flow of $2.4 \cdot 10^{-5}$ m^3/s was released 1.3 m below the surface into an ambient with a stratification of approximately 42 kg/m^4. McDougall's model predicted a separation level of about 45 cm beyond the point of release, while his data revealed a level of about 60 cm.

Since no established and accurate model of this peeling or uncoupling effect has been extensively tested and developed, we adopted a simple peeling model to allow for a continuous plume. This model can use different criteria as a key to change values of $\Delta\rho_{w,m}$, b, and U from what would otherwise be calculated from the conservation equations. As the total plume momentum approaches zero, the magnitude of the derivatives of b and U increase rapidly. Thus these values may serve as one basis for uncoupling. A more physically-based criteria, however, may be found in the use of the total average buoyancy, i.e. an uncoupling occurs when the average buoyancy becomes negative, or has fallen below some ratio of positive to negative buoyancy.

In modeling this peeling process, we considered *when* an uncoupling would occur

and *how much* of the plume water would be lost. Uncoupling will likely occur near the point at which the *average* buoyancy becomes negative and the plume begins to loose momentum. If nothing happens here, the model will predict that the plume quickly reaches zero velocity. We have therefore made the approximation that a peeling event will occur whenever the negative buoyancy of the water has a greater magnitude than the positive buoyancy of the bubbles. When such an event occurs, it is likely that water from the outer portions of the plume will be shed, while the isolated, high-momentum water in the center will remain. We have approximated this partial loss with three simple assumptions: 1) one half of the volume flux of water will be lost, 2) one half of the momentum flux of the water will be lost, and 3) the loss of this water will reduce the centerline density difference of the water, $\Delta\rho_{w,m}$, by fifty percent. Using the Gaussian velocity profile, this loss of mass and momentum flux result in new values of velocity and width such that $b_{\text{new}} = b_{\text{old}}/\sqrt{2}$ and $U_{m,\text{new}} = U_{m,\text{old}}$.

This model, when run to duplicate McDougall's experiments, gives results similar to McDougall's double-plume model, which show an uncoupling occurring before such a phenomenon is physically observed in his experiment. The experimentally observed uncoupling, furthermore, occurs at an elevation past that at which the plume model would predict zero velocity. A possible explanation for this discrepancy is that some of the denser liquid has actually left the plume structure prior to this point through a more-continuous peeling or eddy-shedding process. While an entrainment coefficient based on volume conservation could simply consider the *net* influx of liquid, the impacts of density differences would require a lower effective entrainment coefficient of negative buoyancy. This effect may be responsible for the comparatively low values of α reported by Rayyan (1974) calibrated against the performance of a plume in a stratified ambient environment.

2.3.5 Initial Conditions

Very close to the CO_2 release point, the liquid has no vertical motion except in the wakes of individual bubbles. This momentum is quickly diffused such that at some height above the release, x_e, all of the liquid between the bubbles is moving

vertically. At this height, the flow is considered *established*, such that the property profiles are approximately similar along the length of the plume, and the integral model is applicable. Implementation of this model requires estimation of values of b, U_m, and $\Delta\rho_{w,m}$ at the beginning of the zone of established flow. The distance of flow establishment, x_e, has been roughly estimated as 5D, where D is the port diameter [Milgram 1983]. Note that a single port most likely will be constructed such that the release area is covered by many smaller orifices to decrease the bubble or droplet size. Up until this height, we may assume the effects of stratification are negligible and initially $\Delta\rho_{w,m} = 0$. To determine initial conditions for the evaluation of the equations, an analytic solution was used which assumes that the plume originates from a point source with an initial buoyancy flux which remains constant during the short span of flow establishment. Similar assumptions were used by Cederwall and Ditmars (1970), and Rayyan (1974).

These theoretical approximations for $U_{m,o}$ and b_o at the beginning of the zone of established flow of the modeled release are determined by:

$$b_o = \frac{6}{5}\,\alpha\, x_o \tag{2.31}$$

and

$$U_{m,o} = \left[\frac{25\, g q_{rel}\,(1+\lambda_1^2)}{24\,\alpha^2\pi}\right]^{1/3} x_o^{-1/3} \tag{2.32}$$

where x_o is the distance to established flow from the virtual point source. Near the virtual source, $b \to 0$ and $U_m \to \infty$, such that the virtual source actually lies below the physical release. We will make the approximation that $x_o \approx 2x_e \approx 10$D. Although these values are very approximate, the downstream plume conditions are insensitive to the initial conditions as we demonstrate in the discussion of model sensitivity. Other investigators [Milgram 1983, Chesters *et al.* 1980] have also examined the issue of conditions at the beginning of the zone of established flow for bubble plume modeling, making somewhat different, but equally rough, approximations.

Because x_e is generally small compared to the height of the plume, and within the bounds of uncertainty of the model, we will not consider this additional distance

in evaluation of the rise heights of the plume. Furthermore, it is of the order where effects of port orientation and structure may be realized. For example a release oriented downward may assemble into a developed plume below the "release depth." Thus this distance serves no real purpose other than in the rough determination of initial conditions.

2.3.6 CO_2 Accumulation

The rate of mass transfer of the CO_2 from a bubble or droplet into the surrounding water, as discussed previously, is dependent upon the ambient CO_2 concentration of the surrounding water. Initially, the ambient concentration of about 0.1 kg/m^3 [Riley and Skirrow 1975] is negligible compared to the saturation concentration expected at the CO_2 interface. As CO_2 dissolves into the ambient water, however, the increase in ambient concentration would tend to slow the rate of mass transfer. To examine the magnitude of this effect, we assumed that the *dissolved* CO_2 increase above ambient levels, ΔC_d, also follows a Gaussian distribution such that

$$\Delta C_d = \Delta C_{d,m} e^{-R^2/(\lambda_d b)^2} \tag{2.33}$$

The dissolved CO_2 mass flux is represented by

$$\int_0^\infty \Delta C_d 2\pi U R \, dR = U_m \Delta C_{d,m} \pi b^2 \frac{\lambda_d^2}{1+\lambda_d^2} \tag{2.34}$$

where λ_d is the spreading ratio of the dissolved CO_2 which is approximately λ_2 for a fully dissolved species. Conservation of total CO_2, therefore, may be used to calculate an expression for the increase in dissolved levels within the plume by assuming the total mass flux at any depth is equal to the flux at the release

$$\Delta C_{d,m} = [q_{\text{rel}} \rho_{\text{rel}} - q_z \rho] \left[\frac{1+\lambda_d^2}{U_m \pi b^2 \lambda_d^2} \right] \tag{2.35}$$

As seen in Figure 2-14, however, the magnitude of this increase is on the same order of the ambient level. This figure shows the centerline dissolved concentration considering

a 133 kg/s flow from a single port. Because initially smaller bubbles will dissolve faster, the concentration increase will be higher, but still well below solubility levels. Thus we may conclude that $C_s \gg C_\infty$ and thus assume $C_s - C_\infty \simeq C_s$.

This analysis also assumes that there is a sufficient ambient current to supply a fresh entrainment flow to the plume and to remove CO_2-enriched water which has been shed. This assumption is discussed further in Chapter 4.

2.4 Numerical Solution

Equations (2.4), (2.28), (2.29), and (2.30) were solved numerically by means of a fourth-order Runge-Kutta algorithm based on functions developed in Press *et al.* (1988). The program consisted of four principal functions: 1) a main function which controls input and output and calls secondary functions, 2) an integrator function which performs the fourth-order Runge-Kutta integration, 3) a derivatives function which solves for the values of the separate differential equations, and 4) an ambient condition function which returns values of ambient conditions and CO_2 properties at a given elevation following the two synthetic profiles. To allow for determination of ambient gradients and the input of the slip velocity, a constant, user-input distance step was used for each run ranging from 0.1 to 1.0 m depending on the sensitivity required by the initial conditions. With the exception of model instability occurring at the initialization of the plume for some initial conditions and larger distance steps, long-distance results converged at a step size of less than 1.0 m. The program was run on an M.I.T. Project Athena Digital VAXstation 3100. A complete, annotated listing of the model is presented in Appendix B.

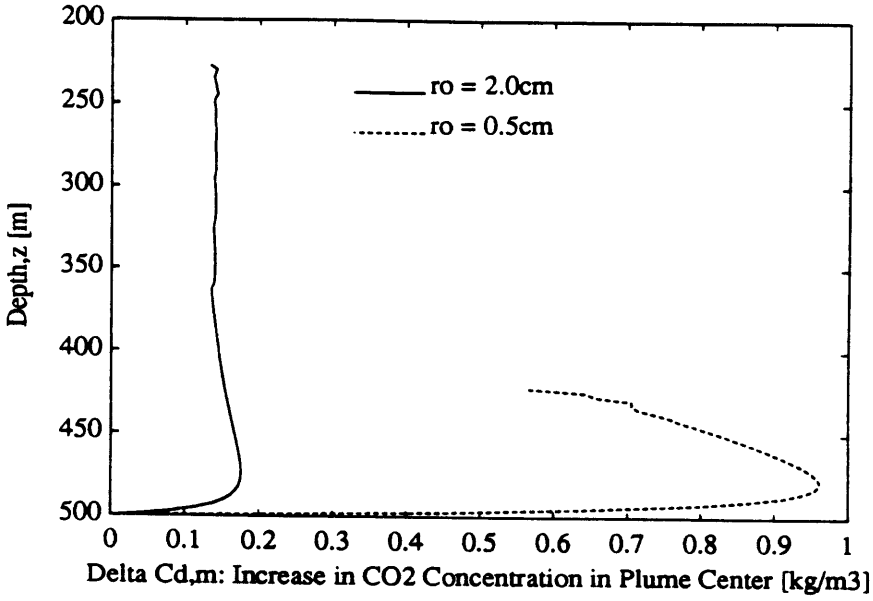

Figure 2-14: Increase in dissolved CO_2 concentration in plume center.

Chapter 3

Model Results

The primary function of this model is to determine the effectiveness of a deep ocean CO_2 release as a means of isolating CO_2 from the atmosphere under a variety of site and facility design variables. Implementing the model requires *a priori* designation of values of α, λ_1, λ_2, γ, functions for U_b and K, as well as estimates of the initial conditions. As stated previously, we have chosen a base set of parameters such that $\alpha = 0.1$, $\lambda_1 = 0.8$, $\lambda_2 = 1.25$, and $\gamma = 1.0$, and have chosen expressions for U_b, K, U_o, and b_o as described in Chapter 2. In addition, we have adopted the high-gradient ocean profile. Appendix A describes the model sensitivity to these choices, as well as the ambient gradient and the peeling/uncoupling model. Briefly, the appendix indicates sensitivity to choices made concerning α and K, while the other parameters and functions are much less sensitive. Variation over possible values of α leads to differences of $\pm$ 25% of the maximum height of the plume, variation of K leads to differences of $\pm$ 35%, while variation of the other parameters leads to differences within $\pm$ 5%. We have adopted values which we feel are physically representative while remaining conservative. In addition, we make the assumption that there is sufficient ambient current to allow for dispersion of the CO_2 after it is shed, as discussed further in Chapter 4.

After adopting a set of consistent parameters and functions to model a release of CO_2 we may now determine the effects of variations in prototype design parameters. In designing a release facility, we may alter four principal variables: (1) the depth

of release, z_o, (2) the local rate of release, i.e. the number of ports, N, on a large diffuser delivering a fixed flow, (3) the initial bubble size, r_o, and (4) the initial plume width, b_o. Note that the designation of a local release rate assumes that a diffuser will contain a number of separate ports which will discharge plumes which must be spaced sufficiently far so as to assure independent behavior. In the limit of decreasing this port spacing, the plume may be analyzed as a line source, rather than as a point source. Also, the initial bubble size and plume width are dependent upon the characteristics of the orifice of the discharge port, and thus these two parameters may not be totally independent. Furthermore, a sufficient flow or pressure may be required to discharge bubbles of a given size, and so there is a relationship between bubble size and the number of ports. For analytical purposes, however, we will assume that these parameters are generally in dependent.

Figure 3-1 shows the plume behavior given a flow rate of 133 kg/s (i.e. from a single 500 MW plant) and a fixed number of bubbles, i.e. fixed initial mass per bubble for a variety of release depths. In this and other figures we examine the centerline plume velocity, U_m, the nominal half width of the plume, b, and the bubble or droplet radius, r, as a function of depth. These variables best represent the behavior of the release. Varying the release depths results in three categories: 1) The CO_2 will totally dissolve prior to reaching 500 m and thus will be in a liquid phase throughout; 2) the CO_2 release will be above 500 m and thus the CO_2 will exist as a vapor; and 3) the CO_2 will be released as a liquid, but will undergo a phase change prior to its complete dissolution.

Each plume has three important heights. The first or deepest is the height at which the average buoyancy becomes negative; it is near this point that we believe CO_2-enriched fluid from the plume will first peel off (uncouple) and horizontally settle. This height may be seen as the first constriction of plume width in the middle Figure 3-1. Further constrictions represent repeated peeling events. Note that the length scales of the horizontal and vertical axes are different, resulting in distortion of the apparent height and width ratio. Next is the point at which all of the CO_2 has dissolved and there are no bubbles remaining, seen in the bottom Figure 3-1 as the

depth at which $r = 0$. At this point there is no longer any positive buoyancy. Shortly afterwards, the third height is reached at which the plume velocity falls to zero and the remaining water settles, seen in the top Figure 3-1 at the depth at which $U_m = 0$. This is the maximum height at which we expect any CO_2 to reach. Note that the last two heights are essentially indistinguishable in Figure 3-1 and in similar figures. Figure 3-1 reveals that a liquid release of the same number of bubbles as an equivalent vapor release requires a longer net distance to dissolve. While the liquid rises more slowly, the increased surface area of the vapor bubbles increases mass transfer such that the total distance to dissolution is somewhat less for bubbles.

Figure 3-2 shows the performance resulting from a 133 kg/s flow of a vapor release at 500 m with variations in the initial bubble radius. Because the buoyancy of the bubbles is the sole source of upward momentum, the total rate of CO_2 dissolution can strongly affect the plume behavior. Because a collection of many smaller bubbles has a higher surface area than the same volume of larger bubbles, they will go into solution more rapidly. In addition, this decreases the buoyancy faster and serves to slow the plume. Thus the maximum height of the plume can be significantly controlled by the initial bubble size. The ability to accurately control this initial size, however, requires further research.

Figure 3-3 shows the performance given varying flows for a vapor release from 500 m. Assuming a base flow of 133 kg/s, we demonstrate the impacts on the resulting plume if the total flow is divided into 5, 10, or 50 parts. If sufficiently spaced, each plume can be assumed to be independent of the others. Note that each case has a different initial velocity based on Equation (2.32), although we have shown that the downstream performance is insensitive to this difference. The size of the plume is highly sensitive to the initial buoyancy flux, and thus splitting the flow among a number of different ports spaced along a diffuser will have a noticeable impact on the maximum height of the plume. This factor, furthermore, may be easily varied at an incremental cost which is small compared to the total pipeline.

The effects of variations in the initial width are seen in Figure 3-4. Differences in initial width tend to impact the behavior of the plume such that a wider plume

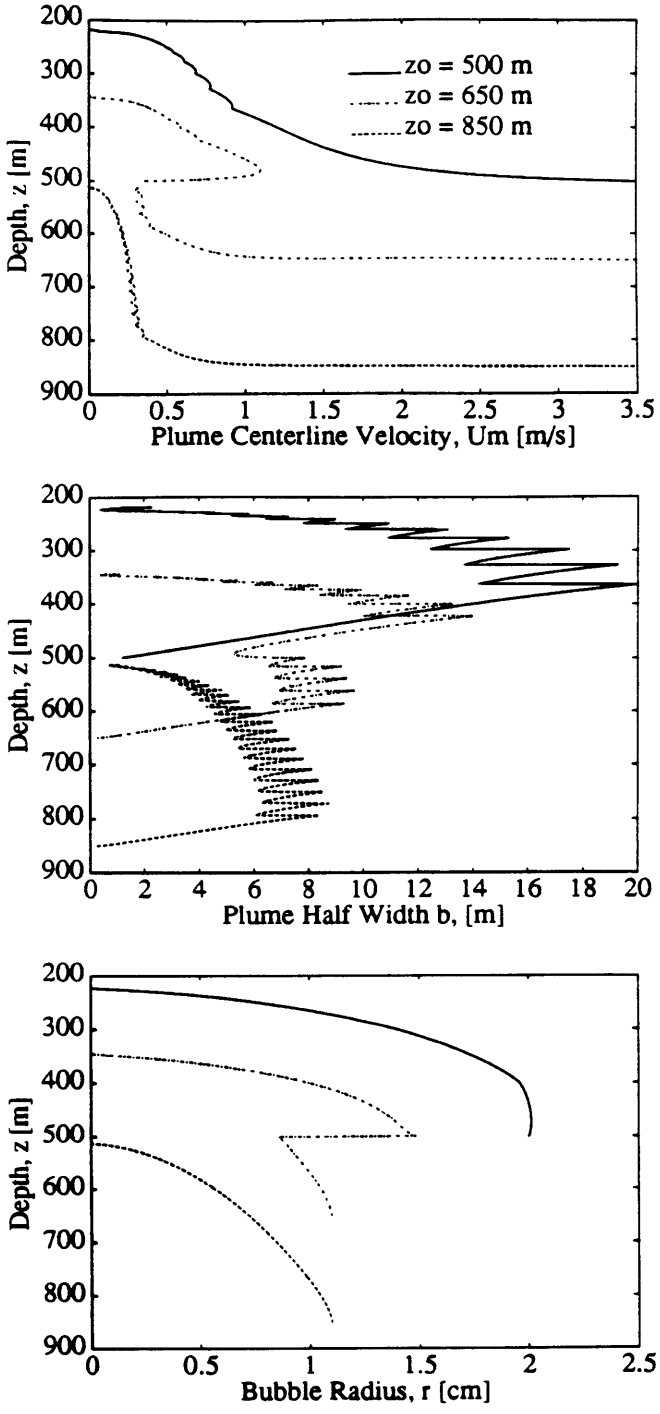

Figure 3-1: Sensitivity to release depth given a 133 kg/s flow and fixed initial bubble and droplet mass.

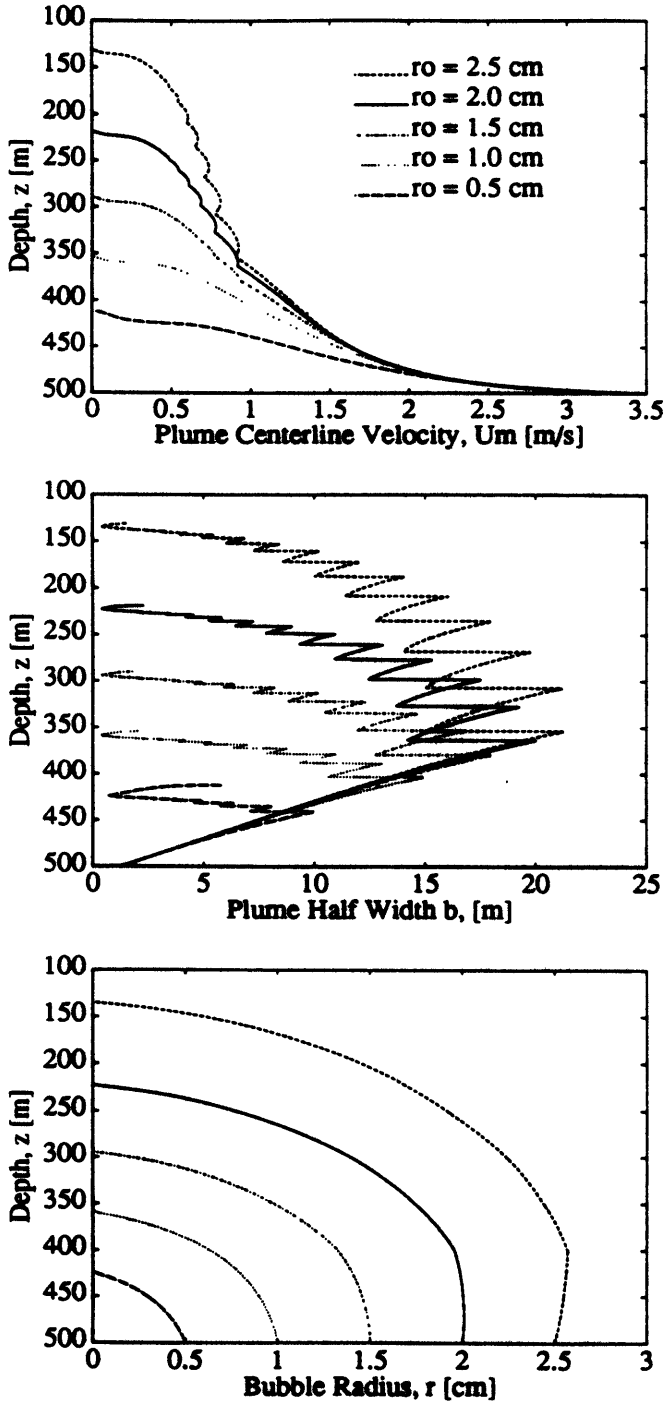

Figure 3-2: Sensitivity to initial bubble size for a 133 kg/s flow released as vapor at 500 m.

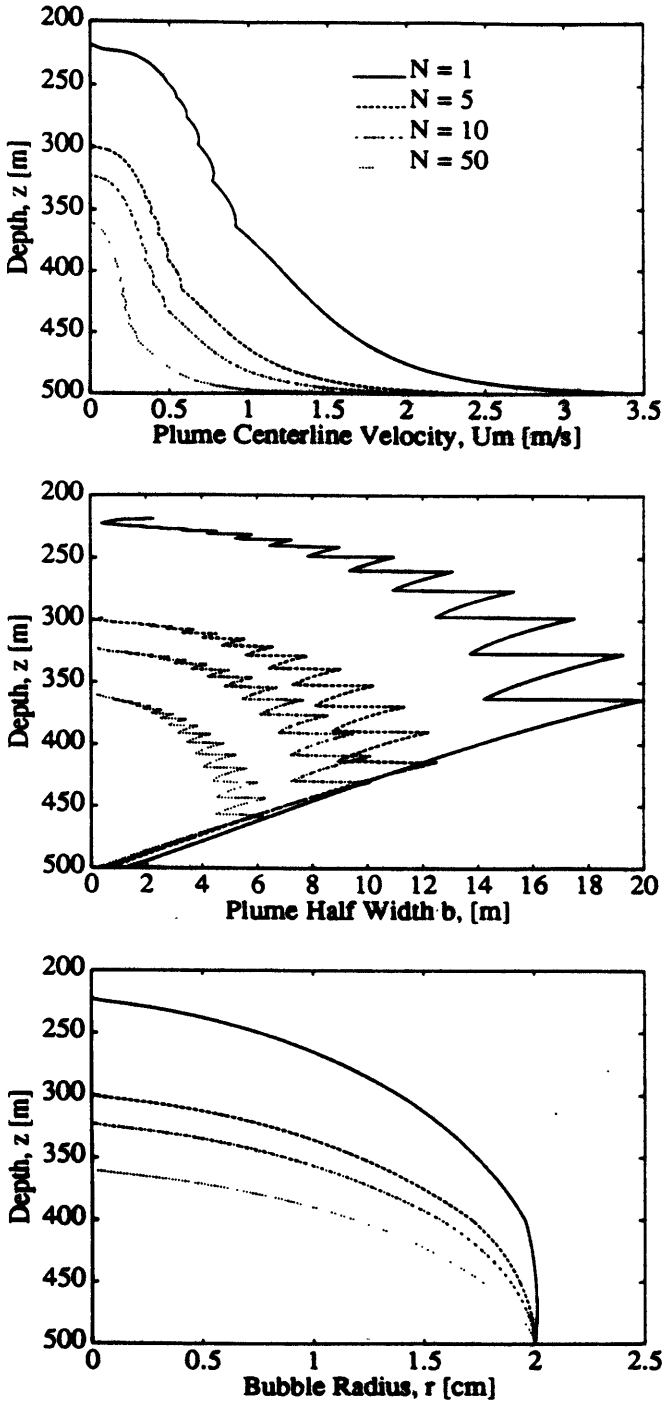

Figure 3-3: Sensitivity to flow variation, i.e. number of ports, for a vapor release from 500 m.

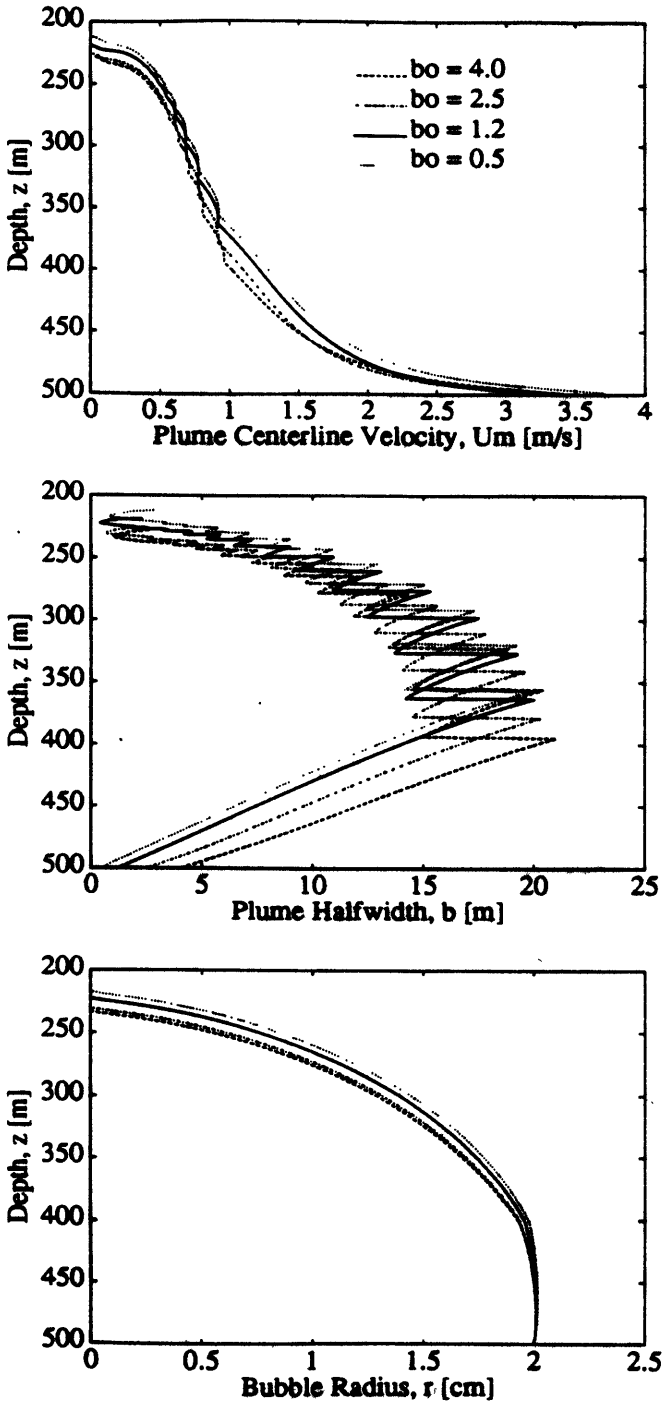

Figure 3-4: Sensitivity to initial plume width for a 133 kg/s flow released as vapor at 500 m.

results in slower velocities which in turn decreases the plume height. This variation, to some degree may be seen as associated with Equation (2.31); a higher initial width may imply a larger x_o. This initial width of the outlet port is variable within the restraints of the facility design; i.e. a diffuser at the end of a release port will initially spread the plume to a greater width. This sensitivity, however, is much less than the effects of varying flow and bubble radius. Thus these latter criteria should be most emphasized within a total diffuser design.

The results (maximum plume height and height of initial uncoupling) of the major design choices are shown in Table 3.1 for a 500 m release depth and in Table 3.2 for an 800 m release depth, both assuming a high ambient density gradient. Because of uncertainties involving hydrate formation, miscibility, and solubility, as well as errors associated with the smaller density difference between liquid CO_2 and sea water, greater uncertainty exists within the modeled projections from the 800 m release. These tables show the *height*, x, to initial uncoupling and the maximum height of upward water velocity for different combinations of r_o and N. We also present calculations for the case of $N \rightarrow \infty$, i.e. there is no induced plume flow and each bubble rises at its slip velocity. This sets a minimum rise height for each bubble size. Figure 3-5 uses these data and shows contours of constant maximum plume height as a function of r_o and N for a release from 500 m.

In addition, the relative impacts of release depth are seen in Table 3.3 which gives the maximum height of the plume, for bubbles or droplets of identical initial mass, as a function of release depth, z_o, and number of ports, N. Table 3.3 indicates that performance improves slightly when increasing release depth for both vapor and liquid releases. Sensitivity is greatest for small values of N and z_o and is due to the effects of pressure and temperature on CO_2 density and solubility. Initial conditions were made assuming a CO_2 release velocity similar to that produced given a port diameter D=1 m and N=1 for a 500 m release (see Section 2.3.5). This implies that for a release at a given depth the total release area, $\pi D^2 N/4$, is constant and that for changes in depth, the total release area is scaled by the density ratio. This analysis shows that significant reductions in these heights may be achieved for low r_o and large N.

r_o [cm] N	2.5	2.0	1.5	1.0	0.5
1	369 / 147	281 / 137	210 / 121	146 / 97	88 / 60
5	261 / 90	201 / 86	150 / 78	104 / 65	61 / 41
10	232 / 73	178 / 70	131 / 65	91 / 54	51 / 35
50	187 / 45	141 / 44	102 / 42	68 / 37	23 / 15
∞	124 / NA	89 / NA	59 / NA	35 / NA	15 / NA

Table 3.1: Maximum plume height [m] *over* height of initial uncoupling [m] for a vapor release from 500 m as a function of initial bubble radius and number of ports.

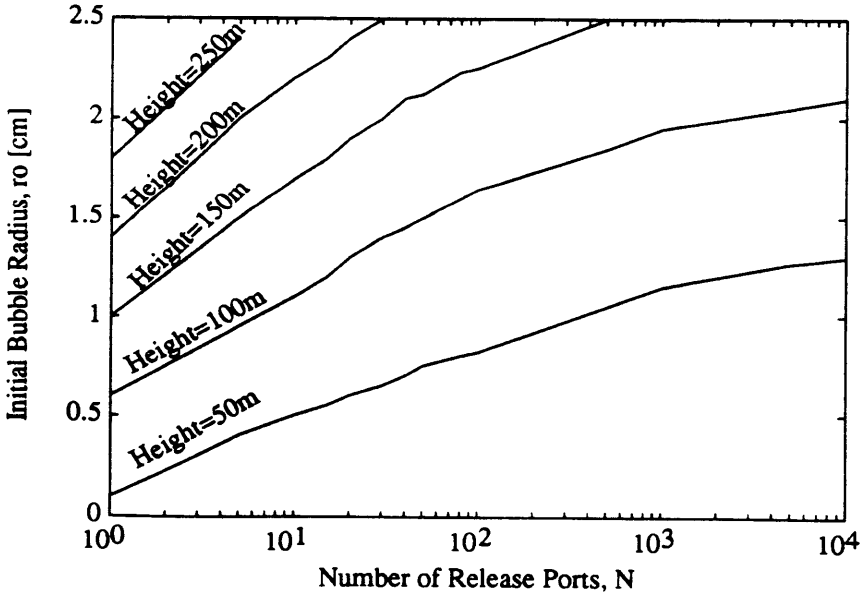

Figure 3-5: Maximum plume height [m] as a function of r_o and N for a 500 m release depth.

r_o [cm] N	1.4	1.1	0.84	0.56	0.28
1	436 60	341 60	244 60	156 56	84 45
5	342 40	244 40	174 40	110 37	57 30
10	310 32	217 32	154 32	96 31	49 27
50	238 20	168 20	116 20	70 20	34 18
∞	136 NA	74 NA	55 NA	20 NA	10 NA

Table 3.2: Maximum plume height [m] *over* height of initial uncoupling [m] for a liquid release from 800 m as a function of initial droplet radius and number of ports. Note that the columns represent droplets of identical mass to the bubbles in Table 3.1 (i.e. a droplet of $r_o = 1.4$ cm at 800 m has the same mass as a bubble of $r_o = 2.5$ cm at 500 m).

z_o [m] r_o [cm] N	300 1.33	400 1.16	500 1.00	650 0.57	800 0.56	1000 0.55
1	176	153	146	166	156	152
5	118	106	104	114	110	108
10	100	91	91	98	96	93
50	70	68	68	71	70	67

Table 3.3: Maximum height of plume [m] as a function of release depth and number of ports. All bubbles or droplets have the same initial mass.

Chapter 4

Potential Design

4.1 Diffuser Criteria

As seen in Tables 3.1 and 3.2 a CO_2 release into the deep ocean may be dissolved within a reasonably short distance above the release depth, and this dissolution height may be reduced by controlling the number of ports through which the total stream is released and by reducing the size of the bubbles at the orifice.

These values, however, are based on the assumptions that 1) the multiple plumes behave independently, and 2) that there is a sufficient supply of ambient water. These factors must be considered when developing an appropriate release structure.

Based on a release depth of 500 m such that the CO_2 is released as a vapor, we examine the important design considerations to develop a rough prototype release design. To develop a potential design, we will begin by selecting the number of diffuser ports and the initial bubble size, as these variables can strongly influence the behavior of the plume. Based on Table 3.1, we will adopt a moderate number of diffuser ports such that N = 10 and choose an initial bubble size such that $r_o = 1.0$ cm. While the number of ports may be constructed almost arbitrarily, there is some uncertainty as to the modifications in port and orifice designs required to modify the bubble size. We feel that a value of $r_o = 1.0$, however, is reasonable and may be easily achieved. Our model predicts that under this scenario, the plume will begin to peel CO_2-enriched water beginning about 50 m above the release, and the upward current

of water will be maintained until about 90 m above the release, i.e. $z = 410$ m.

Our first consideration is the dynamic independence of the plumes. The plumes must be separated such that the expanding flows do not intersect and interfere with each other. Our model predicts that each plume will reach a maximum half-width, b, of approximately 10 m immediately prior to the peeling stage. With this criteria, we may initially set the port spacing to be 20 m, and thus the total length of release will be approximately 200 m.

Given this criteria, we now turn to the flow required to supply clean entrained water. Our entrainment hypothesis states that the flow is entrained such that

$$\frac{dQ}{dx} = 2\pi\alpha b U_m \tag{4.1}$$

and this is integrated by the model over the length of the plume to determine the total rate of entrained flow, Q_e. Our model predicts that each plume will entrain water at a rate of about 140 m^3/s, and thus the total rate of the ten plumes will be 1400 m^3/s. The entrainment flow must be able to reach the plumes, and the diluted CO_2-enriched water must be transported away without significant re-entrainment. As shown in Figure 4-1, two limiting conditions are possible. Under conditions of forced convection, characterized by high ambient current speeds, entrainment is supplied from upstream by an ambient current which also transports the CO_2-enriched water downstream. Under conditions of free convection, characterized by weak current speeds, entrainment approaches the plume as a sink flow induced by the low pressure at the plume edges. The enriched, shed water is then transported radially outward, at a higher elevation, as a density current. Similar regimes have been recognized in conventional plumes, but bubble plumes present a complication due to the peeling process. Note that in the second case, the thickness of the internal spreading layer must adjust itself to accommodate the required flow and as a result may limit the height over which the plume can entrain fresh ambient water. An approximate criterion for the ambient current speed, V_a, required to cause a transition between the two regimes may be calculated as follows. We define the ambient cross flow as the

product of the ambient current, V_a, and the projected frontal area of the plume array, A, estimated as the height, about 90 m for our case, multiplied by the width, 200 m. Based on this criteria, we may calculate a minimum V_a as

$$V_a > \frac{Q_e}{A} \approx \frac{1400 m^3/s}{18,000 m^2} \approx 0.08 m/s \tag{4.2}$$

This criteria assumes that entrainment is continuous along the length of the plume, and does not sufficiently account for the CO_2-enriched water which is intermittently shed and may be subject to re-entrainment in the upper portion of the plume. Examining CO_2 mass conservation, however, we may determine the minimum cross current necessary to remove the mass of dissolved CO_2 by forced convection. This criteria requires that the mass input, $\dot{M}$, of 133 kg/s is matched by an outward mass flux from the local ambient water. This outward flux is estimated by taking the product of an average CO_2 dissolved concentration and a cross flow based on an area, A', based on the height from the initial uncoupling to the maximum plume height, i.e. 40 m for this release. This represents the area over which the CO_2-enriched water will be shed. The average concentration may be estimated as $\dot{M}/Q_e$, which may be verified against maximum values obtained by Equation (2.35). This design gives $\Delta C_d = 0.09 kg/m^3$

Accordingly,

$$V_a > \frac{\dot{M}}{\Delta C_d A'} \approx \frac{130 kg/s}{\left(0.09 kg/m^3\right)\left(8,000 m^2\right)} \approx 0.18 m/s \tag{4.3}$$

While some sites may feature ambient currents in excess of 0.18 m/s, inducing forced convection, it is more likely that the currents will be less. For example, measurements by Schuert (1970) taken at a depth of 300 m in the north Pacific and discussed subsequently, averaged about 0.1 m/s. For such smaller currents, entrainment and outward transport will be regulated in part by free convection. Depending on the density gradient, which affects the ability of a density current to transport the enriched water, some re-entrainment could take place, effectively raising the ambient concentration. Because of the very large solubility, however, this increase will have

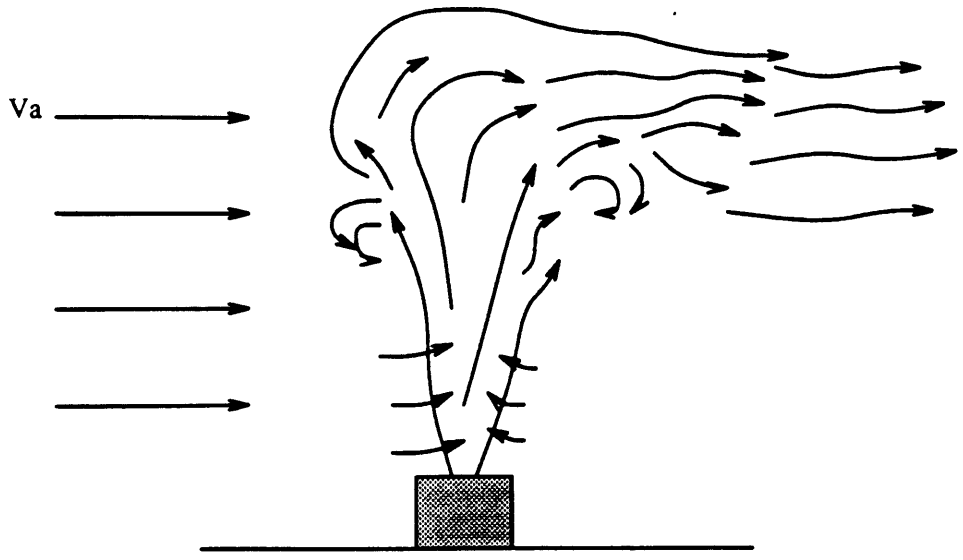

Forced Convection, Large Va

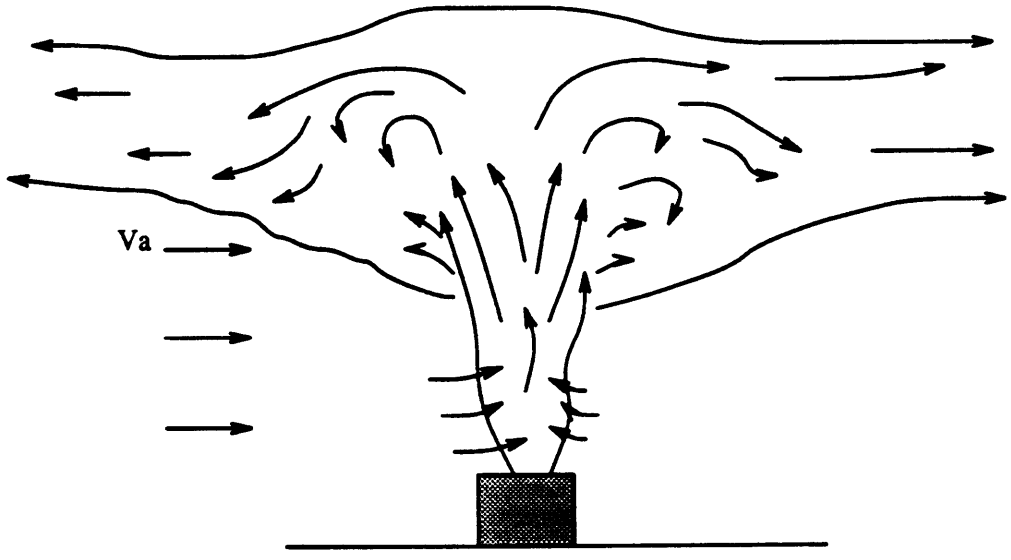

Free Convection, Small Va

Figure 4-1: Limiting conditions of ambient entrainment and transport of CO_2-enriched water in a stratified ambient.

little impact on the ability to dissolve CO_2. As a best guess, we may assume that re-entrainment leads to a factor of two increase in CO_2 concentration, or about 0.2 kg/m^3. As an extremely conservative scenario, we may assume $V_a = 0.01$ m/s, ignore the density current altogether, and calculate an equilibrium ambient concentration increase from Equation (4.3) such that $\Delta C_{d,a}$=1.5 kg/m^3. Although this is a relatively large increase compared to the normal background levels ($\sim$ 0.1 kg/m^3), it is still much less than solubility concentrations ($\sim$ 40 kg/m^3) such that mass transfer will not be significantly impeded.

Though we have modeled the entire flow of 133 kg/s as being composed of CO_2, other trace constituents are present as seen in Table 1.1. These substances will also enter solution, and should be diluted according to their fraction of the full flow as predicted by the model. For our best guess CO_2 concentration increase of 0.2 kg/m^3, the resulting concentration increase of N_2 and O_2 is about 0.01 kg/m^3. Similarly, the resulting concentration increase of SO_2 is about 10^{-3} kg/m^3, and NO_x $2 \cdot 10^{-4}$ kg/m^3.

These constituent concentrations are very small, and it is likely that any local chemical impacts will be dominated by the CO_2. This CO_2 will tend to make the receiving water more acidic, titrating the bicarbonate buffer system [Golomb *et al.* 1989]. This effect will be counteracted by the dissolution of natural carbonate particles that descend from the surface layer. The plume and pH adjustment are likely to have only local and minor biological effects. Specific impacts, however, particularly regarding the possibility of hydrate formation and precipitation, should be more closely examined.

In the intermediate vicinity of the release, the predominantly horizontal currents will disperse the CO_2 and other constituents in the direction of flow. To consider possible impacts beyond the near-field region, we may estimate a down stream distance, $L_{\frac{1}{2}}$, such that concentrations will be diluted by a factor of two due to horizontal dispersion, as

$$L_{\frac{1}{2}} = \frac{3}{2} \frac{w^2 V_a}{K_h} \tag{4.4}$$

where w is a lateral plume length scale related to a Gaussian distribution and ap-

proximately equal to one-fourth the total width of the diffuser array, and K_h is a horizontal diffusivity. Using this expression, taking $K_h = 0.1\,m^2/s$ from dye measurements conducted by Schuert (1970) at a depth of 300 m in the north Pacific, and assuming V_a = 10cm/s, and w = 50 m, then $L_{\frac{1}{2}} \approx 4$km. The plume will also be diluted by vertical diffusion, but vertical diffusion coefficients are typically several orders of magnitude smaller than horizontal coefficients. Because the height and width of the intermediate field are comparable, vertical diffusion will be much less effective.

4.2 Economics of Capture and Disposal

A preliminary capital cost estimate for a 500 MW coal-fired power plant retrofit with air separation/flue gas recycling for ocean disposal is $366 million of which $79 million is due to ocean disposal (see Table 4.1). The costs of ocean disposal can vary greatly due to accessibility to a suitable disposal site. These estimates reflect a pipeline of 160 km and a release depth of 450 m. Also, we assume that there will be no harmful environmental problems associated with releasing CO_2 that would add additional costs.

While the electricity cost will vary in different locations, for the sake of analysis we will take the cost of electricity for a 500 MW coal-fired power plant as about 46 mills/kWh. Of this, 18 mills/kWh is for the fuel, while the remainder is the capital charge plus operating and maintenance costs. When a CO_2 capture system is retrofit to this plant, the net power output is reduced because of the parasitic power required to capture the CO_2. For an air separation/flue gas recycling plant, the CO_2 capture system requires about 30% of the plant's output. This derating of the plant raises the cost of electricity from 46 mills/kWh to 65 mills/kWh. The cost and operation of the capture and compression system adds another 18 mills/kWh and the disposal system another 6 mills/kWh. This results in a total cost of 89 mills/kWh for electricity production with CO_2 capture, or about twice current prices.

Component	Cost (10^6 \$)
O_2 Plant (10,000 tons/day)[a]	135
CO_2 Compressor[b]	38
Other[c]	53
CO_2 Disposal[d]	79
Contingency[e]	61
Total	366

[a]Golomb, et al. 1989

[b]Golomb, et al. 1989

[c]Other includes cost of piping for CO_2 recycle, dehydration system, etc. (Golomb, et al. 1989)

[d]Based on a 160 km pipeline with a release depth of about 450m [Smelsor et al. 1990]

[e]A 20% contingency factor is used.

Table 4.1: Capital cost estimate of 500 MW coal-fired power plant retrofit for air separation/flue gas recycling and ocean CO_2 disposal.

Chapter 5

Long-Term Fate

Though the principal objective of this research was to investigate the buoyancy and mass-transfer effects present in the near-field region of a CO_2 release, this is useful only within the context of the implications of far-field transport.

The effectiveness of any deep-ocean CO_2 discharge ultimately depends upon the vertical transport of the CO_2. If the aim of the facility is to keep the CO_2 out of the atmosphere, then any transport back toward the atmosphere would be counter-productive. The most obvious application of this idea can be seen within the plume itself. If the bubbles have not all dissolved prior to reaching the bottom of the upper mixed layer at about 100 m then this gas will obviously quickly find its way into the atmosphere due to equilibrium pressures. Similarly, any CO_2-enriched water that has reached the upper layer will lose the CO_2 to the atmosphere. While these dynamic transport concerns may be easily addressed in the diffuser design, there are also large-scale oceanographic transport phenomena which serve to carry the dissolved CO_2 back up toward the atmosphere.

The subject of vertical transport of CO_2 within the ocean has received considerable attention principally with the intent of modeling the rate of *downward* transport into the ocean as a result of increased atmospheric levels. Focusing on the upward vertical movement, however, is somewhat different in that transport of local regions of CO_2-enriched water involves site-specific considerations. Global circulation in an ocean basin (e.g., North Pacific) consists of the formation of deep cold water at the poles

which is advected vertically downward and horizontally toward the equator where it is upwelled [Sverdrup *et al.* 1942]. Hence net vertical transport due to this circulation depends on latitude. In addition to this large-scale circulation, small-scale, local turbulent transport also takes place. This complex circulation and vertical transport may be modeled, though in a highly parameterized manner, with an eddy diffusivity model. A characteristic value of vertical eddy diffusivity beneath the surface mixed layer is of order $K_z = 1\,cm^2/s$ [Veronis, 1969] or about 3000 m^2/year. Transport within the surface mixed layer is considerably more vigorous, so once CO_2 has diffused into the mixed layer, it will exchange rapidly with the atmosphere. Assuming that the depth of the well-mixed layer is approximately 100 m, that the CO_2 from the bubble plume is trapped at a depth Z_T beneath the surface, and ignoring vertical upwelling, the time scale for exchange to the atmosphere is of order

$$\mathcal{T} = \frac{(Z_T - 100)^2}{K_z} \tag{5.1}$$

Using the above estimate for K_z, the calculated time scales are shown in Figure 5-1. Note that for CO_2 trapped between depths of 400 and 500 m, i.e. a vapor release from 500 m, the associated time scale to atmospheric mixing will be on the order of 30 to 50 years. For a trap depth of 900-1000 m, i.e. a liquid release from 1000 m, the time scale will be on the order of 200 to 300 years. While clearly approximate, these calculations show that the characteristic residence time of CO_2 injected into the ocean is finite.

Additional analyses have been performed by other investigators. Hoffert *et al.* (1979) used a large-scale ocean diffusion model to estimate the comparative impacts of releasing varying portions of the fossil-fuel CO_2 increase into the ocean at a number of depths. This did not take into accounts the local effects associated with a single discharge, but rather examined the general implications of vertical transport. He concluded that no matter how effective the discharge may be, the final *very long-term* atmospheric levels over time will not be reduced by ocean injection. Highly effective ocean disposal, however, may be able to reduce the peak levels by about 50

per cent, and may be able to delay the increase by several hundred years. Figure 5-2 shows his projections of atmospheric levels for a variety of scenarios. A review of this subject, which also examines factors such as biotic uptake and mineral buffering, may be found in de Baar and Stoll (1989).

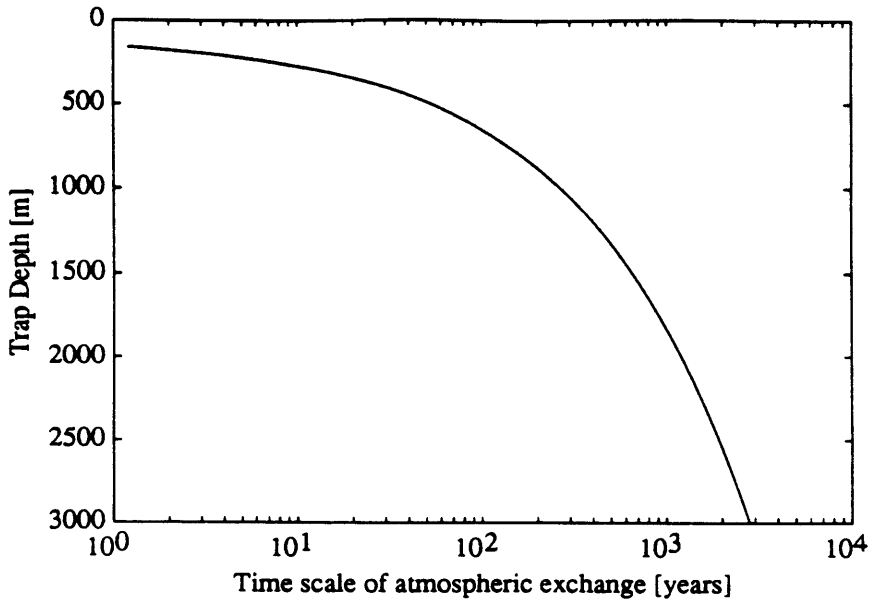

Figure 5-1: CO_2 Time scales for atmospheric exchange

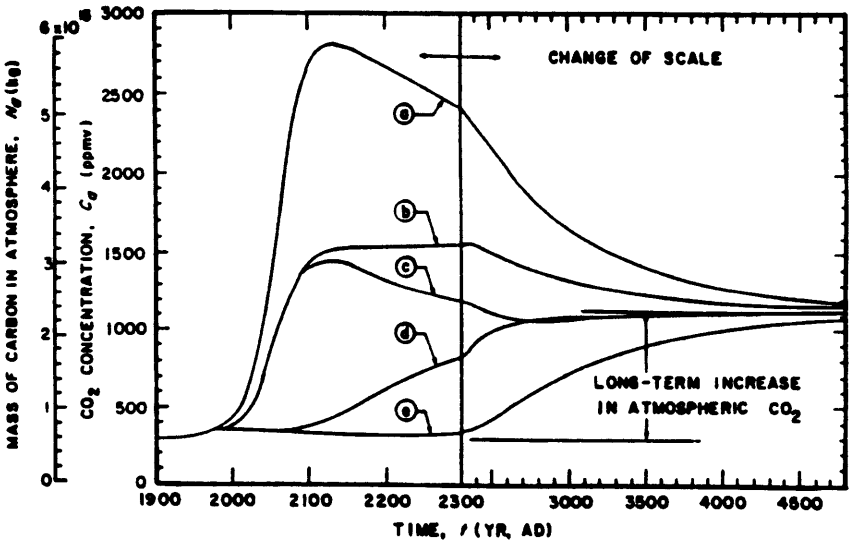

Figure 5-2: Model projections of atmospheric CO_2 variations assuming entire fossil fuel reserve is depleted as a logistic function of time: (a) 100% injected into the atmosphere, (b) 50% injected at oceanic depth of 1500 m and 50% into the atmosphere, (c) 50% injected at sea floor (4000 m) and 50% into atmosphere, (d) 100% injected at oceanic depth of 1500 m, (e) 100% injected at sea floor (4000 m). All oceanic injections initiated in 1985. Note five-fold compression in time-scale beyond 2300. [Hoffert *et al.* 1979]

Chapter 6

Conclusions and Recommendations

6.1 Conclusions

1. A release of CO_2 into the deep ocean in quantities associated with a 500 MW coal-fired power plant may be easily dissolved into seawater. For depths less than about 500 m, the CO_2 will be in a vapor state, while for lower depths the CO_2 will be in a liquid state and the formation of CO_2-hydrates is possible. For release depths less than 3000 m, the CO_2 will be positively buoyant and will rise toward the surface, inducing an upward plume. The size and height of this plume may be decreased by releasing the flow through an increased number of ports of a multi-port diffuser and/or by decreasing the initial size of the CO_2 vapor bubbles or liquid droplets.

2. Using a multi-port diffuser with 10 ports and an initial bubble radius of 1 cm, complete dissolution can occur within about 100 m above the release point for the vapor phase. For a liquid release, a similar dissolution height with a 10 port diffuser requires droplets with an initial radius of about 0.5 cm.

3. Using the same diffuser configuration, concentration increases of CO_2 SO_2, and NO_x near the plume will be about 0.2 kg/m^3, $1 \cdot 10^{-3}$ kg/m^3, and $2 \cdot 10^{-4}$ kg/m^3 respec-

tively. Given an ambient current of 10 cm/s, horizontal dispersion will dilute these concentration increases by a factor of two at a distance of about 4 km downstream.

4. Long-term vertical ocean transport phenomena will dictate the ultimate effectiveness of a release; simple calculations suggest that a release from a 500 m depth will begin to re-enter the atmosphere within a time-scale of 30 to 50 years and a release from 1000 m will begin to re-enter within a time-scale of 200 to 300 years. These residence times may be increased by releasing in areas of ocean downwelling or by the formation of solid CO_2-hydrates.

5. Implementing a CO_2 capture and sequester scheme based on a retrofit air separation/flue gas recycling coal-fired power plant, given a 160 km pipeline for release at a depth of 450 m, will approximately double the electricity cost.

6.2 Recommendations for Future Research

Our modeling relies upon a number of assumptions which may be uncertain. In order to provide a more certain model of a deep-ocean CO_2 release, we suggest further research and examination of a number of issues.

1. Solubility and Stability of Liquid CO_2 in Deep Ocean Conditions

Below approximately 500 m, CO_2 will exist as a liquid in equilibrium with the ambient temperature and pressure. Under these conditions, i.e. high pressure and low temperature, the physical behavior of the CO_2 is somewhat uncertain. We have assumed immiscible droplets and a constant, conservative approximation of the solubility. Previous solubility experimentation on CO_2 at these conditions, however, has been unable to produce consistent data due to the formation of hydrates and the miscibility of CO_2 under certain conditions. The rate of mass transfer will vary with the magnitude of CO_2 solubility, so the determination of more exact dissolution times will require more precise understanding of the solubility. If the liquid CO_2 is

times will require more precise understanding of the solubility. If the liquid CO_2 is in fact miscible with seawater, furthermore, the situation would be more similar to a conventional plume than the unique features of a bubble plume. A miscible release in a highly stratified ambient, for example, would quickly loose its buoyancy and spread at a much lower level than a similar flow of droplets.

2. CO_2-Hydrate Formation

A similar question involving the physical behavior of CO_2 at these depths surrounds the formation of hydrates. While the formation of hydrates under these conditions has been observed, the exact nature of the formation is uncertain. Formation involves kinetic and seeding considerations which are uncertain in a deep ocean environment. Because hydrates may potentially be able to transport CO_2 to the ocean bottom because of their negative buoyancy, a release scenario to enhance their formation may significantly improve the long-term effectiveness. However, the possibility that hydrates could clog the delivery line and diffuser ports complicates the design. Further examination of the physical chemistry involved is required to obtain an accurate representation of these effects.

3. Plume Peeling Effects

An additional point of uncertainty involves the peeling or uncoupling of negatively buoyant water from the core of a bubble plume in a stratified environment. This phenomenon most likely is a combination of continuous peeling along the length of the plume, accompanied by intermittent, discrete large-scale uncoupling events as observed in McDougall's (1978) experiments. A related question concerns how the CO_2-enriched water is transported away from the plume, as a density current, under conditions of weak ambient current. Because these processes affect the local fate of the CO_2-enriched water, more certain predictions may be made with greater understanding of the physical processes. We do note that by decreasing the initial local flow of CO_2 (through the use of more diffuser ports) and bubble size, uncertainty associated with the peeling effect may be diminished.

4. Orifice Design

We have assumed that the release orifice may be designed to produce bubbles much smaller than the maximum dynamically allowable size. In order to achieve this effect, the release must occur under conditions creating a shattered or atomized flow, or must be split among a great number of smaller orifices such that the local release flow is small enough that single bubbles form at the opening. The latter case is unlikely given the very large flows encountered. The nature of flow shattering at the orifice, therefore, or some other means of physical disruption, must be better understood prior to the development of a design requiring small initial bubble size.

5. Far field considerations of local releases

To a large degree, the long-term fate of any released CO_2 is dependent upon the oceanographic transport phenomena of the local release region. A release into a sinking or downwelling region, for example, would have a significantly longer, though still finite, residence time in the ocean than a release into an upwelling region. To better understand the effectiveness of any particular site, therefore, requires an examination of the local physical oceanography.

6. Environmental Impacts

Finally, the CO_2 will modify the local chemical balances in the region of the release, will create intense local vertical transport, and may perhaps form large amounts of solid hydrate. The environmental impacts of these, and perhaps other, effects should be further studied prior to development.

Chapter 7

References

Albanese, A. S. and M. Steinberg, *Environmental Control Technology for Atmospheric Carbon Dioxide*, DOE/EV-0079 (1980).

Aybers, N.M. and A. Tapucu, "Studies on the Drag and Shape of Gas Bubbles Rising through a Stagnant Liquid", *Wärme-und Stoffübertragung* 2, 171-177 (1969).

Baddour, R. E., "Computer Simulation of Ice Control with Thermal-Bubble Plumes – Line Source Configuration", *Canadian Journal of Civil Engineering*, v.17, 509-513 (1990).

Baes, C. F. Jr., S. E. Beall, D. W. Lee, and G. Marland, *Options for the Collection and Disposal of Carbon Dioxide*, ORNL-5657 (1980).

Bialek, Eugene L., *Handbook of Oceanographic Tables*, U.S. Naval Oceanographic Office, Washington D.C., 60 (1966).

Boussinesq, J., "Calcul du Pouvoir Refroidissant des Courants Fluids", *J. Math. Pures et Appliques* 6, 285 (1905).

Bulson, P. S., "The Theory and Design of Bubble Breakwaters", *Proceedings of the Coastal Engineering Conference*, London, 995-1015 (1968).

Cederwall, K. and J. D. Ditmars, "Analysis of Air-Bubble Plumes", California Institute of Technology W. M. Keck Laboratory of Hydraulics and Water Resources,KH–R–24 (1970).

Chesters, A. K., M. van Doorn, and L. H. J. Goossens, "A General Model for Unconfined Bubble Plumes from Extended Sources", *International Journal of Multiphase Flow*, v.6, 499-521 (1980).

Clift, R., J. R. Grace and M. E. Weber, *Bubbles, Drops, and Particles*, Academic Press, New York, (1978).

Cussler, E. L., *Diffusion: Mass Transfer in Fluid Systems*, Cambridge University Press, Cambridge, England (1984).

de Baar, Hein J. W. and Michel H. C. Stoll, "Storage of Carbon Dioxide in the Oceans", *Climate and Energy: The Feasibility of Controlling CO_2 Emissions*, P. A. Okken, R. J. Swart and S. Zwerver (eds.), Kluwer Academic Publishers, Dordreicht, 143-176 (1989).

Fannelop, T. K. and K. Sjoen, "Hydrodynamics of Underwater Blowouts", *Proc. AIAA, 18th Aerospace Science Meeting*, Pasadena, California (1980).

Godon, A. M. and J. H. Milgram, "Mixing of Fluids in Tanks by Gas Bubble Plumes", *Journal of Fluids Engineering*, v.109, 186-204 (1987).

Golomb, D., H. Herzog, J. Tester, D. White, and S. Zemba, "Feasibility, Modeling and Economics of Sequestering Power Plant CO_2 Emissions in the Deep Ocean", Massachusetts Institute of Technology Energy Laboratory, MIT–EL 89-003 (1989).

Goossens, Louis H. J. and John M. Smith, "The Hydrodynamics of Unconstrained Bubble Columns for Mixing Lakes and Reservoirs", *Chemical Engineering Technology*, v.47, 951 (1975).

Hendriks, C., K. Blok, and W. Turkenburg, "Technology and Cost of Recovering and Storing Carbon Dioxide from an Integrated Combined Cycle," University of Utrecht, Department of Science, Technology and Society (1990).

Hoffert, Martin I., Y-C. Wey, A. J. Callegari, W. S. Broeker, "Atmospheric Response to Deep-Sea Injections of Fossil-Fuel Carbon Dioxide", *Climatic Change*, 2, 53-68 (1979).

Houghton, G., A. M. McLean and P. D. Ritchie, "Compressibility, Fugacity, and Waer-Solubility of Carbon Dioxide in the Region 0-36 atm. and 0-100°c", *Chemical Engineering Science*, v.6 132-137 (1957).

Hu, S. and R. C. Kinter, "The Fall of Single Liquid Drops Through Water", *A.I.Ch.E. Journal*, v.1,1 42-48 (1955).

Hussain, N. A., and B. S. Narang, "Simplified Analysis of Air-Bubble Plumes in Moderately Stratified Environments", *Journal of Heat Transfer*, v.106, 543-551 (1984).

Jones, Warren, "Air Barriers as Oil-Spill Containment Devices", *Society of Petroleum Engineers Journal;*, 126-142 (1972).

Kobus, H. E., "Analysis of the Flow Induced by Air-Bubble Systems", *Proceedings of the Coastal Engineering Conference*, London, 1016-1031 (1968).

Leitch, A. M. and W. D. Baines, "Liquid Volume Flux in a Weak Bubble Plume", *Journal of Fluid Mechanics*, v.205, 77-98 (1989).

Marchetti, C., "On Geoengineering the CO_2 Problem", *Climatic Change*, v.1, 59-68 (1977).

McDougall, T. J., "Bubble Plumes in Stratified Environments", *Journal of Fluid Mechanics*, v.85,4, 655-672 (1978).

McDougall, T. J., "Negatively Buoyant Vertical Jets", *Tellus*, v.33, 313-320 (1981).

McLellan, H., *Elements of Physical Oceanography*, Permagon Press, Oxford, (1965).

Milgram, J. H., "Mean Flow in Round Bubble Plumes", *Journal of Fluid Mechanics*, v.133, 345-376 (1983)

Milgram, J. H. and R. J. VanHouten, "Plumes from Sub-Sea Well Blowouts", *Proc. 3rd Intl. Conf. BOSS*, v.1, 659-684.

Morton, B. R., Taylor, G. I., and Turner, J. S., "Turbulent Gravitational Convection from Maintained and Instantaneous Sources," *Proceedings of the Royal Society*, v.A234, 1-23 (1956).

Munjal, P. and P. B. Stewart, "Correlation Equation for Solubility of Carbon Dioxide in Water, Seawater, and Seawater Concentrates", *Journal of Chemical and Engineering Data*, v.16,2, 170-172 (1971).

Press, W. H., B. P. Flannery, S. A. Teukolsky, and W. T. Vetterling, *Numerical Recipes in C*, Cambridge University Press, Cambridge (1988).

Rayyan, F. M., "Dynamics of Bubble Plumes Incorporating Mass Transfer", Master's Thesis, The University of Texas at Austin (1972).

Rayyan, F. M., "Hydrodynamics of Bubble Plumes Incorporating Gas Transfer in Stratified Impoundments", Ph.D. Dissertation, The University of Texas at Austin (1974).

Riley, J. P. and G. Skirrow, *Chemical Oceanography*, Academic Press, London, 1-181 (1975).

Rouse, H., C. S. Yih, and H. W. Humphreys, "Gravitational Convection from Boundary Sources", *Tellus*, v.4, 201 (1952).

Sakai, H., T. Gamo, E-S. Kim, M. Tsutsumi, T. Tankaka, J. Ishibashi, H. Wakita, M. Yamano, and T. Oomori, "Venting of Carbon Dioxide-Rich Fluid and Hydrate Formation in Mid-Okinawa Trough Backarc Basin", *Science*, v.248, 1094-1096 (1990).

Schuert, E. A. "Turbulent Diffusion in the Intermediate Waters of the North Pacific Ocean", *Journal of Geophysical Research*, v.75,3, 673-682 (1970).

Smelser, S. C. and G. S. Booras, "An Engineering and Economic Evaluation of CO_2 Removal from Fossil Fuel-Fired Power Plants", Electric Power Research Institute (1990).

Song, K. Y. and R. Kobayashi. "Water Content of CO_2 in Equilibrium with Liquid Water and/or Hydrates", *Society of Petroleum Engineers Formation Evaluation*, 500-508 (1987).

Speece, R. E., *Hypolimnion Aeration with Commercial Oxygen*, EPA-660/2-73-025 (1973).

Steinberg, M. and H. C. Cheng, *Advanced Technologies for Reduced CO_2 Emissions*, BNL-40730 (1987).

Steinberg, M., H. C. Cheng, and F. Horn, *A Systems Study for the Removal, Recovery and Disposal of Carbon Dioxide from Fossil Fuel Power Plants in the U.S.*, DOE/CH/00016-2 (1984).

Stewart, P. B. and P. Munjal, "Solubility of Carbon Dioxide in Pure Water, Synthetic Sea Water, and Synthetic Sea Water Concentrates at -5° to 25° C. and to 10- to 45-Atm. Pressure", *Journal of Chemical and Engineering Data*, v.15,1, 67-71 (1970).

Stommel, H. and K. Yoshida, *Kuroshio: Physical Aspects of the Japan Current*, University of Washington Press, Seattle (1972).

Sun, T-Y. and G. M. Faeth, "Structure of Turbulent Bubbly Jets–I. Methods and Centerline Properties", *International Journal of Multiphase Flow*, v.12,1, 99-114 (1986).

Sun, T-Y. and G. M. Faeth, "Structure of Turbulent Bubbly Jets–II. Phase Property Profiles", *International Journal of Multiphase Flow*, v.12,1, 115-126 (1986).

Sverdrup, H. U, M. W. Johnson, and R. H. Fleming, *The Oceans*, Prentice-Hall, New York, 605-761 (1042).

Taylor, G. I., "The Action of a Surface Current Used as a Breakwater", *Proceedings of the Royal Society*, v.A231 (1955).

Topham, David R., "The Modeling of Hydrocarbon Bubble Plumes to Include Gas Hydrate Formation", *Chemical Engineering Science*, v.39,1, 1613-1622 (1984).

Treyball, Robert E., *Liquid Extraction*, McGraw-Hill, New York, 182-186 (1963).

Tsang, Gee, "Modelling Criteria for Bubble Plumes–A Theoretical Approach", *Canadian Journal of Civil Engineering*, v.11, 293-298 (1984).

Vargaftik, N. B., *Tables on the Thermophysical Properties of Liquids and Gases*, John Wiley and Sons, New York (1975).

Veronis, G., "On Theoretical Models of the Thermocline Circulation", *Deep-Sea Research* v.16 (supplement), 301-323 (1969).

Vukalovich, M. P., and V. V. Altunin, *Thermophysical Properties of Carbon Dioxide*, Collet's Ltd., London (1968).

Weibe, R. and V. L. Gaddy, "The Solubility of Carbon Dioxide in Water at Various Temperatures from 12 to 40° and at Pressures to 500 Atmospheres. Critical Phenomena", *Journal of the American Chemical Society*, v.62, 815-817 (1940).

Weiner, Aaron, "Mass-Transfer From a Gas Rising in a Liquid", Ph.D Dissertation, The University of Pennsylvania (1974).

Weiner, A. and S.W. Churchill, "Mass Transfer from Rising Bubbles of Carbon Dioxide", in D.B. Spaulding (ed.), *Physicochemical Hydrodynamics*, Advance Publications, London, 525-539 (1977).

Appendix A

Model Sensitivity

A.1 Plume Parameter Sensitivity

For our presentation of parameter sensitivity, we have adopted a base scenario such that a full flow of 133 kg/s is released at a depth of 500 m with an initial bubble radius of 2.0 cm. Base parameters were set such that $\alpha = 0.1$, $\lambda_1 = 0.8$, $\lambda_2 = 1.25$, and $\gamma = 1.0$. Equations (2.32) and (2.31) were used with $x_o = 10$ m, based on a release width of about 1 m, such that $U_o = 3.5$ m/s, and $b_o = 1.2$ m. We display results for the high gradient ambient profile. These variations in model performance are qualitatively similar under both synthetic ocean profiles, however. We examine sensitivity by varying a single parameter while holding the others constant.

As discussed in Chapter 2, previous researchers have determined and used different values for the plume parameters α, λ_1, and λ_2. The greatest variation of reported values was for the spreading ratio of the CO_2 volume fraction to the plume velocity, λ_1. This parameter was reported from a low value of 0.2 to a high value of 0.8. Furthermore, the value of this parameter is likely dependent upon the size of the bubbles, and thus may not in fact be constant. As demonstrated in Figure A-1, however, the model was fairly insensitive to changes in λ_1. Note in these figures the effects of the peeling model on the width and velocity of the plume. For further consideration, we adopted a value of $\lambda_1 = 0.8$ which was chosen because it provided more conservative results, and because more-recent investigators [Milgram, 1983] have

suggested errors in the older, lower values. As discussed in Chapter 2, however, the value may be related to bubble size and the large bubbles used in our tests may suggest lower values of λ_1.

The use of a spreading ratio of the water density defect to the plume velocity, λ_2, as a means of incorporating the impacts of the negative buoyancy of the entrained water was limited to Rayyan (1974), who cited a value of 1.25. This value was derived by fitting to a particular entrainment coefficient, and was not explicitly determined. Additionally, temperature spreading in thermal plumes suggests a value of $\lambda_2 \approx 1.1$. We examine the sensitivity of values of λ_2, as seen in Figure A-2. The likely value is somewhat greater than unity, and there is little change in behavior between a value of 1.25 and that of 1.0, i.e. assuming that the density spreads equivalently to the velocity. We will adopt $\lambda_2 = 1.25$ based on Rayyan's calculations for a bubble plume, though the behavior is generally insensitive over the range of likely values.

The performance of the model is rather sensitive to the range of reported values of the entrainment coefficient, α, as shown in Figure A-3. Further consideration of the previous research, however, reveals that the entrainment coefficient tends to increase with buoyancy flux [Milgram 1983, Rayyan 1974]. Furthermore, correlations by Milgram (1983) suggest that α may be as high as 0.15. Because of the uncertainty associated with entrainment in very large plumes, particularly taking water buoyancy effects into consideration, we will adopt a value of $\alpha = 0.1$. This value is high enough to be appropriate to the large scale of the plume, yet may be somewhat conservative if actual values are higher. The sensitivity decreases as the values increase, moreover, such that the variation between $\alpha = 0.1$ and $\alpha = 0.15$ is moderate.

Finally, although the momentum amplification factor, γ, is most likely approximately unity for large-scale plumes, we examine the model sensitivity to this parameter. Milgram (1983) shows experimental data of a wide range of plumes revealing a maximum observed value of $\gamma = 2.8$. Figure A-4 shows that there is little variation between constant values of $\gamma = 1$ and $\gamma = 2$, and that the effects are such that $\gamma = 1$ provides a conservative estimate of the maximum height of the plume.

Thus, we will use constant plume parameters for all stages of the model such that

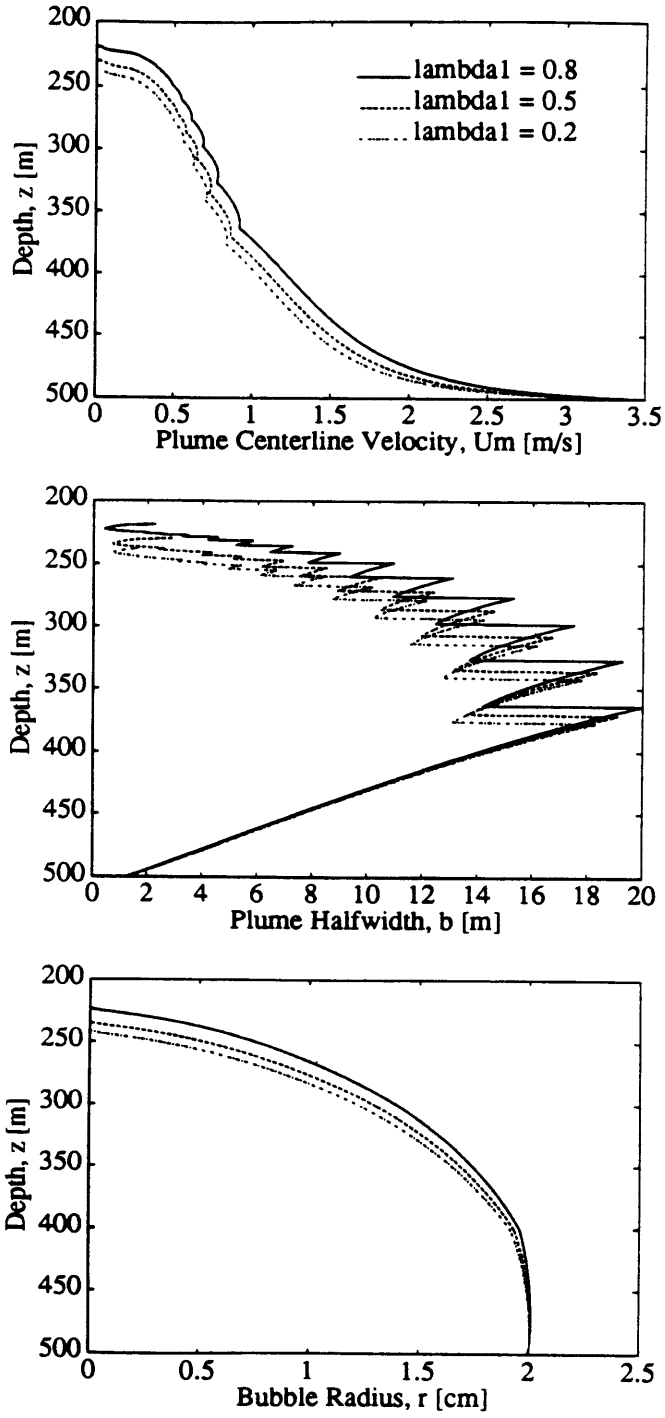

Figure A-1: Sensitivity to λ_1.

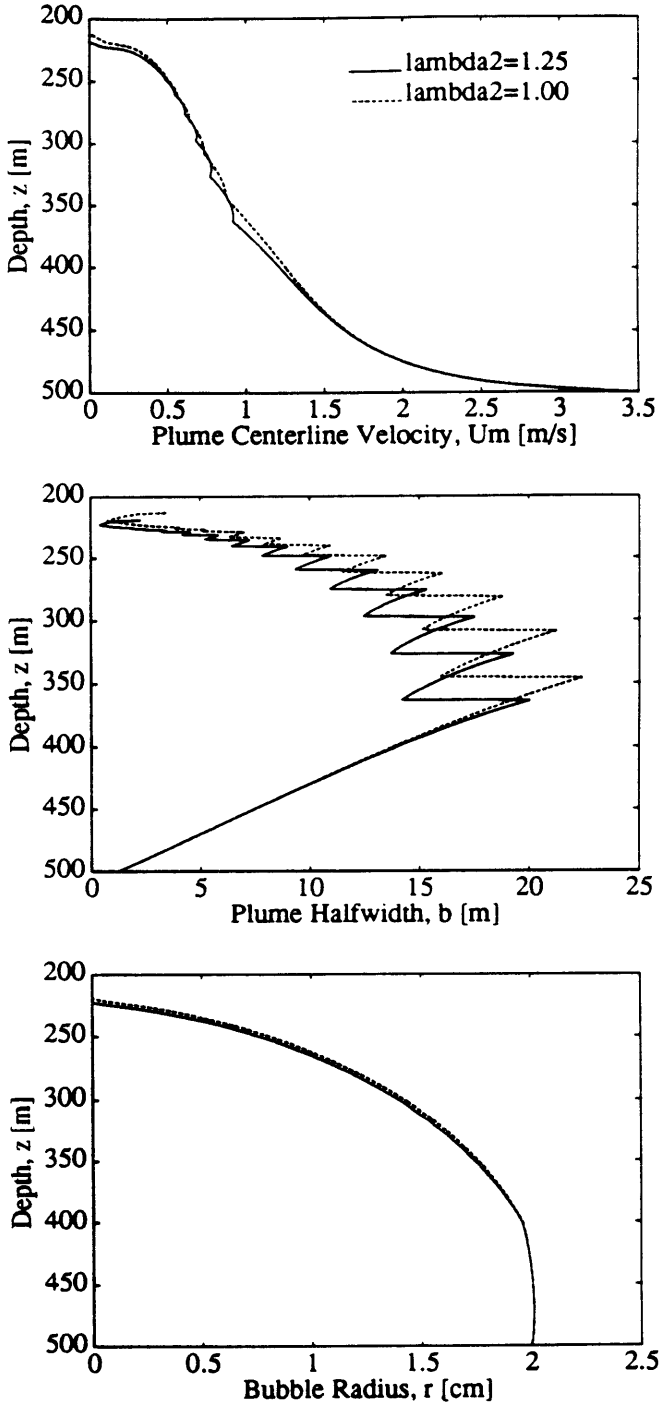

Figure A-2: Sensitivity to λ_2.

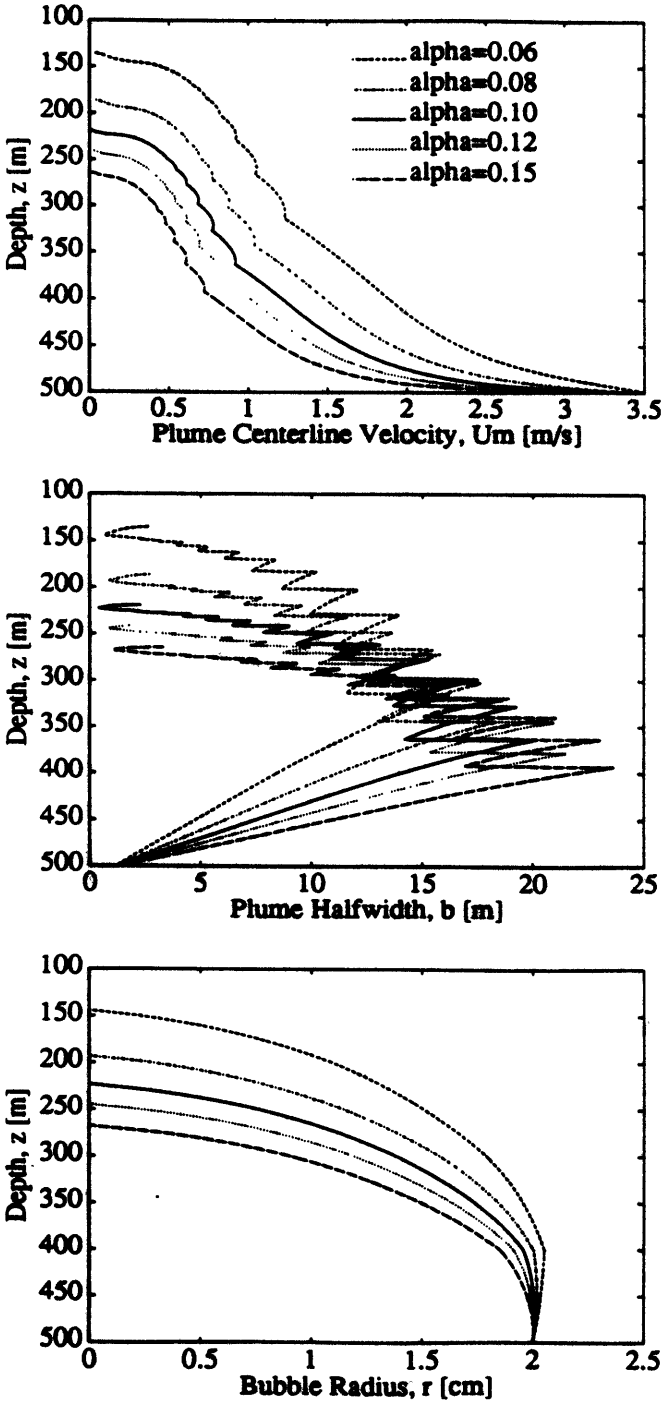

Figure A-3: Sensitivity to α.

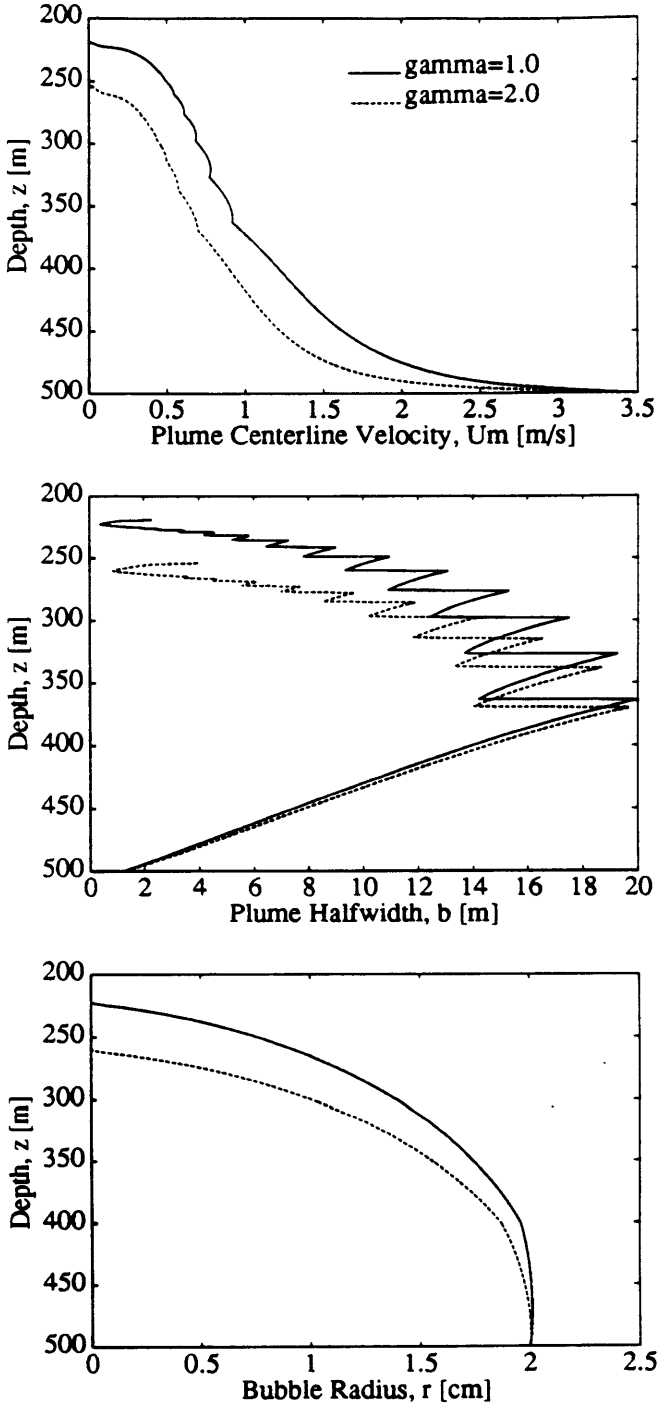

Figure A-4: Sensitivity to γ.

$\alpha = 0.1$, $\lambda_1 = 0.8$, $\lambda_2 = 1.25$, and $\gamma = 1.0$.

Additional sensitivity analysis was performed on the initial conditions of plume centerline velocity, U_m, and width, b. Figure A-5 shows that after about 50 meters from the numerical origin, there is a general convergence in velocity values from a wide range of initial conditions resulting in small differences downstream. Varying the initial value of b, however, does not result in convergence,but rather the values tend to maintain the initial difference as seen in Figure 3-4. As discussed in Chapter 3, varying the initial value of the plume width has a small effect on the performance of the plume, and this variation may be associated with a shift in the height of the beginning of integration.

A.2 Peeling/Uncoupling Model Sensitivity

As described in Chapter 2, our representation of the peeling observed in bubble plumes in a stratified ambient environment assumes that a discrete uncoupling event occurs at heights at which the positive buoyancy is equal in magnitude to the negative buoyancy, and that one-half of the flow, momentum, and negative density difference are shed. Sensitivity to these choices can be seen by examining the condition for peeling, how much water is lost, how much may possibly be re-entrained, and the resulting effects on the momentum.

Figure A-6 shows the results of varying the ratio of negative to positive buoyancy required to peel. If this ratio is infinite in absolute value, then no peeling will occur, and the model will predict a negative plume velocity before all the bubbles have dissolved. It is physically unrealistic that the plume momentum will drop to zero before all the bubbles are dissolved, and this elevation should not be seen as a physical limit of plume motion. Though this criterion logically affects the distance required until the initial uncoupling, the upper limit of the plume is not sensitive to this criteria. As the phenomena is related to the balance of positive and negative buoyancy, we have chosen the point at which they are of equal magnitude as our approximate length.

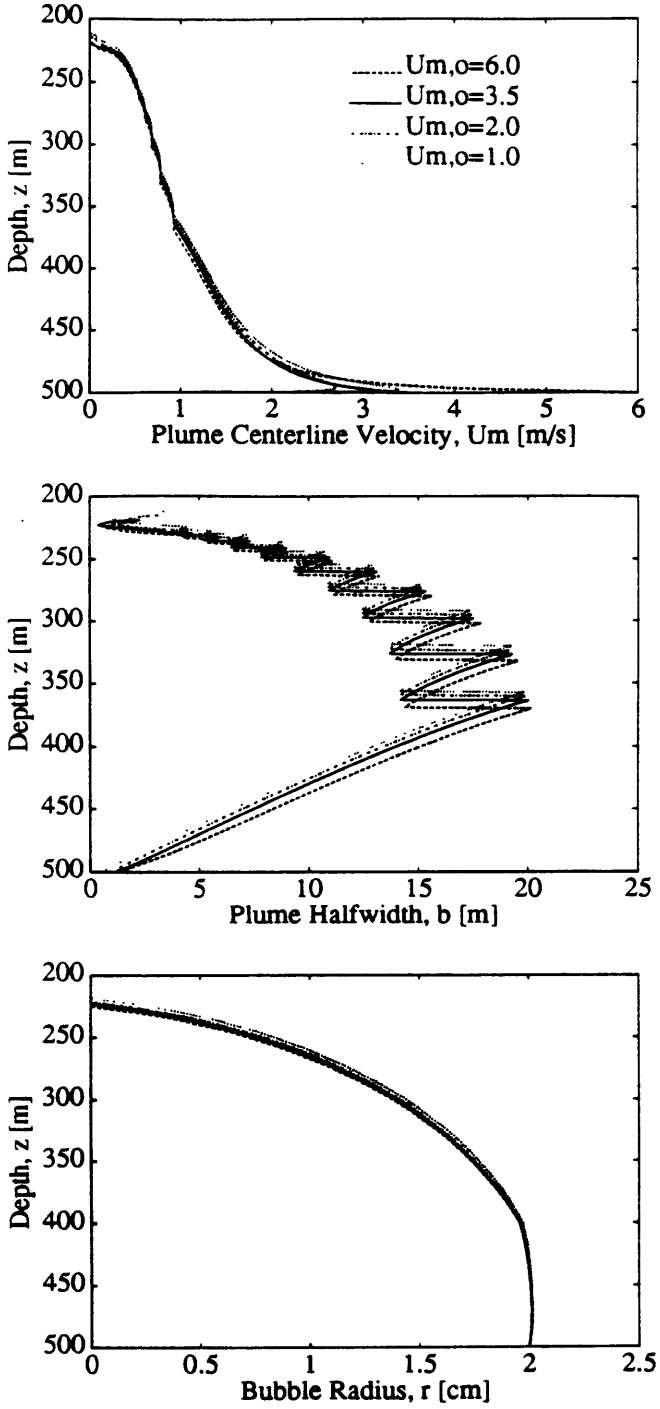

Figure A-5: Sensitivity to initial plume velocity.

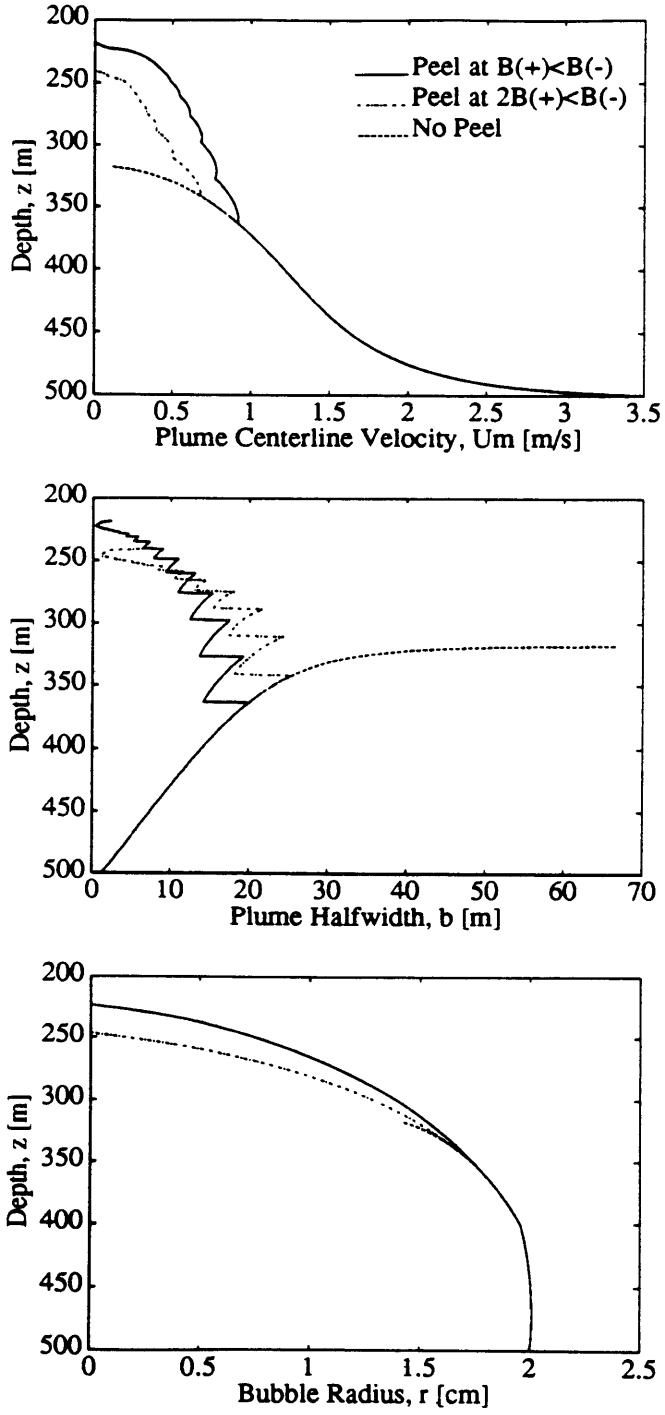

Figure A-6: Sensitivity to peeling criteria.

Figure A-7 shows the results of varying the change in $\Delta\rho_{w,m}$, while flow and momentum are unchanged. These numerical changes imply the physical possibility of entrainment of neutrally buoyant water in connection with the uncoupling, i.e. if the negative buoyancy is decreased while the momentum and mass flow are maintained, an equal volume of fresh water must be instantaneously entrained as the heavy water is shed. Due to the Boussinesq approximation made in the plume model, however, there are few dynamic effects and thus little sensitivity.

Figure A-8 shows the effects of varying the flow and momentum after the uncoupling. In general, the behavior is sensitive to these discrete adjustments; however our simple assumptions appear to be reasonable interpretations of the physical events.

A.3 Bubble Function Sensitivity

Previous researchers have also reported a number of expressions for the slip velocity of a bubble or droplet, U_b, and the mass transfer coefficient, K, for a moving bubble or droplet as discussed in Section 2.2.

Values for the slip velocity of vapor bubbles are well-represented by Equation (2.11); however there is some disagreement between Clift's Equation (2.9) and Treyball's Equation (2.12) regarding the velocity of liquid droplets. Figure A-9 shows the net differences between these two expressions. For the most part, they are similar, though since the Treyball expression does not vary with droplet size, the differences are larger as the bubbles decay. We adopt Equation (2.9) given by Clift for large bubbles because it is a specific representation for the size of bubbles most prevalent in a prototype release and because it incorporates a decrease in velocity with bubble size.

In addition, a range of values for K have been proposed by previous researchers. As can be seen in Figure A-10, the behavior of the model is fairly sensitive to the choice of a mass transfer coefficient. Given this uncertainty, we have adopted Clift's Equation (2.5) to provide more conservative results than Cussler's expression, while still incorporating the effects of a large bubble size which are not taken into account

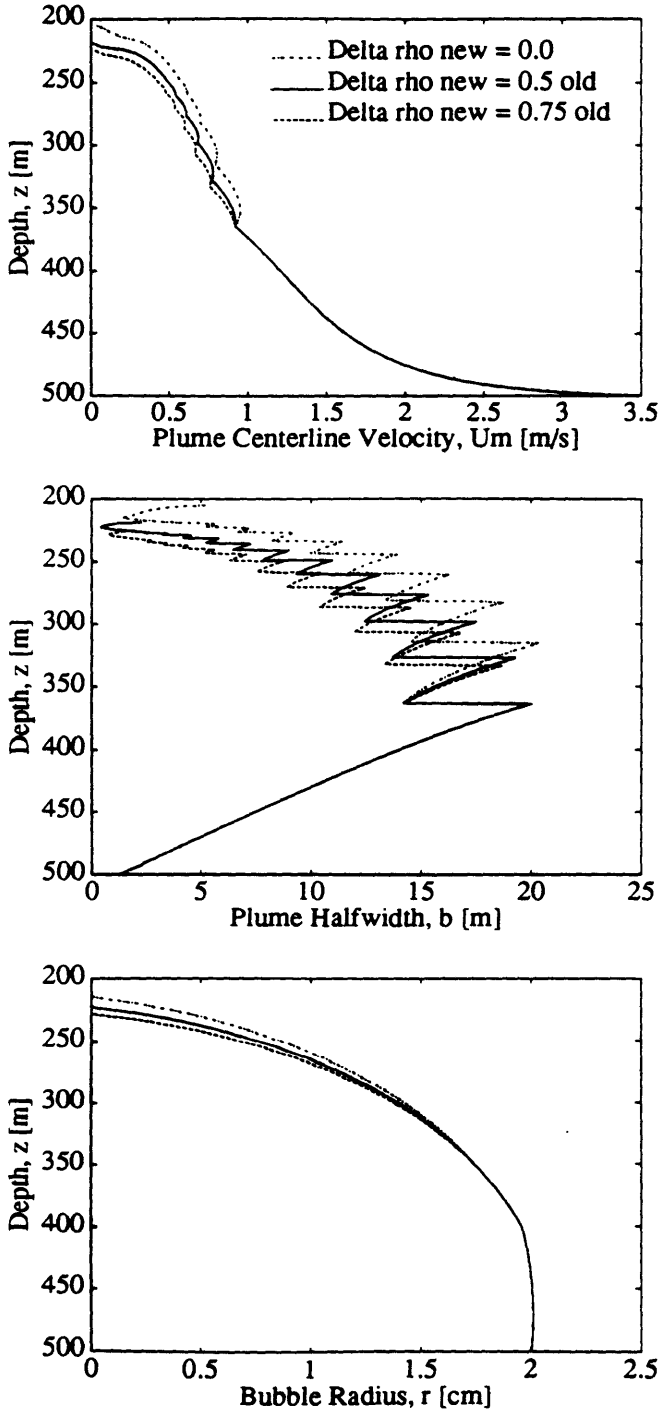

Figure A-7: Sensitivity to magnitude of shed negative buoyancy.

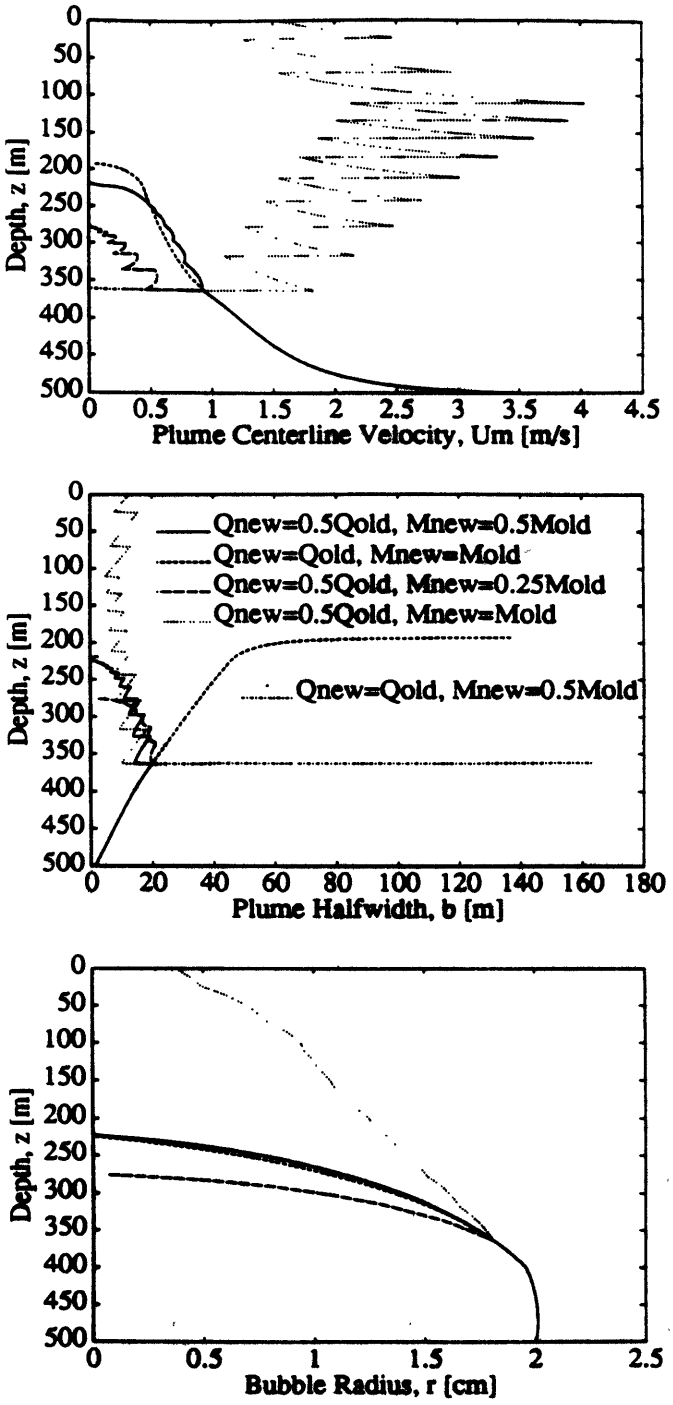

Figure A-8: Sensitivity to shed flow and momentum.

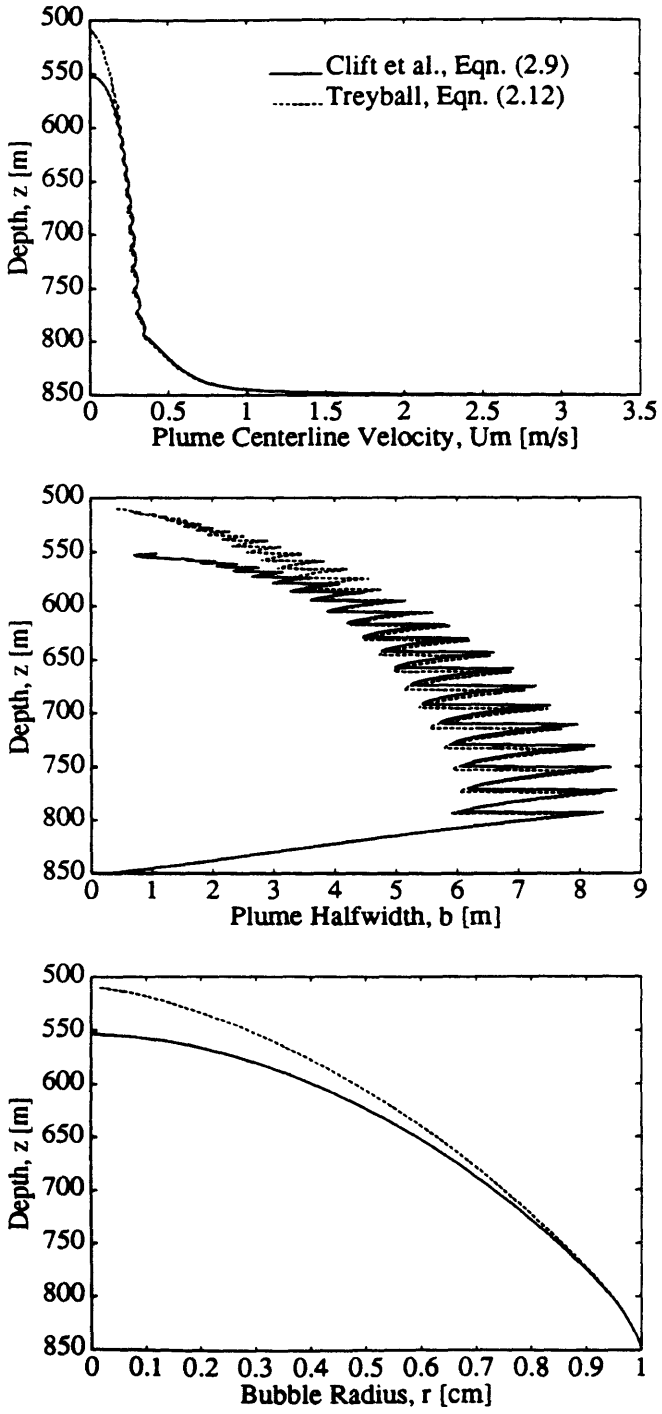

Figure A-9: Sensitivity to U_b formulas for liquid droplets.

in Equations (2.6) and (2.7).

A.4 Ambient Gradient Sensitivity

Figure A-11 shows the sensitivity to the ambient conditions. A steep gradient tends to decrease the distance to the first peel, and requires the plume to peel more frequently. The maximum height of the plume, however, is not sensitive to the ambient gradient.

A.5 Summary

Model results are insensitive to most of the assumptions and parameter choices. Heights to bubble or droplet dissolution vary by less than $\pm$ 5% over the range of likely choices. Exceptions are the entrainment coefficient α, the mass transfer coefficient K, and certain elements of the gradient and peeling effects. Variation in α leads to differences of $\pm$ 25% of our base calculations, and variation of K leads to differences of $\pm$ 35%. Our parameter and function choices, however, would all appear to be generally representative of values offered in the literature or conservative, in the sense of increasing the height of CO_2 dissolution.

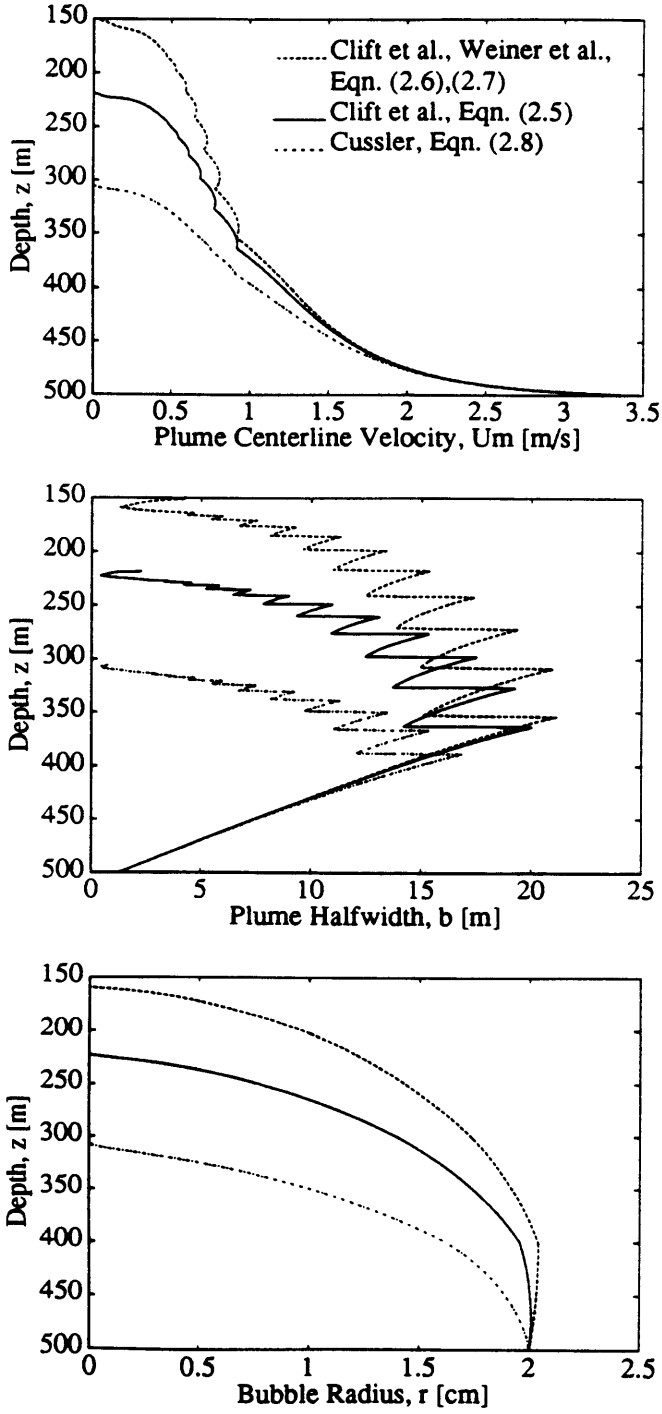

Figure A-10: Sensitivity to K formulas.

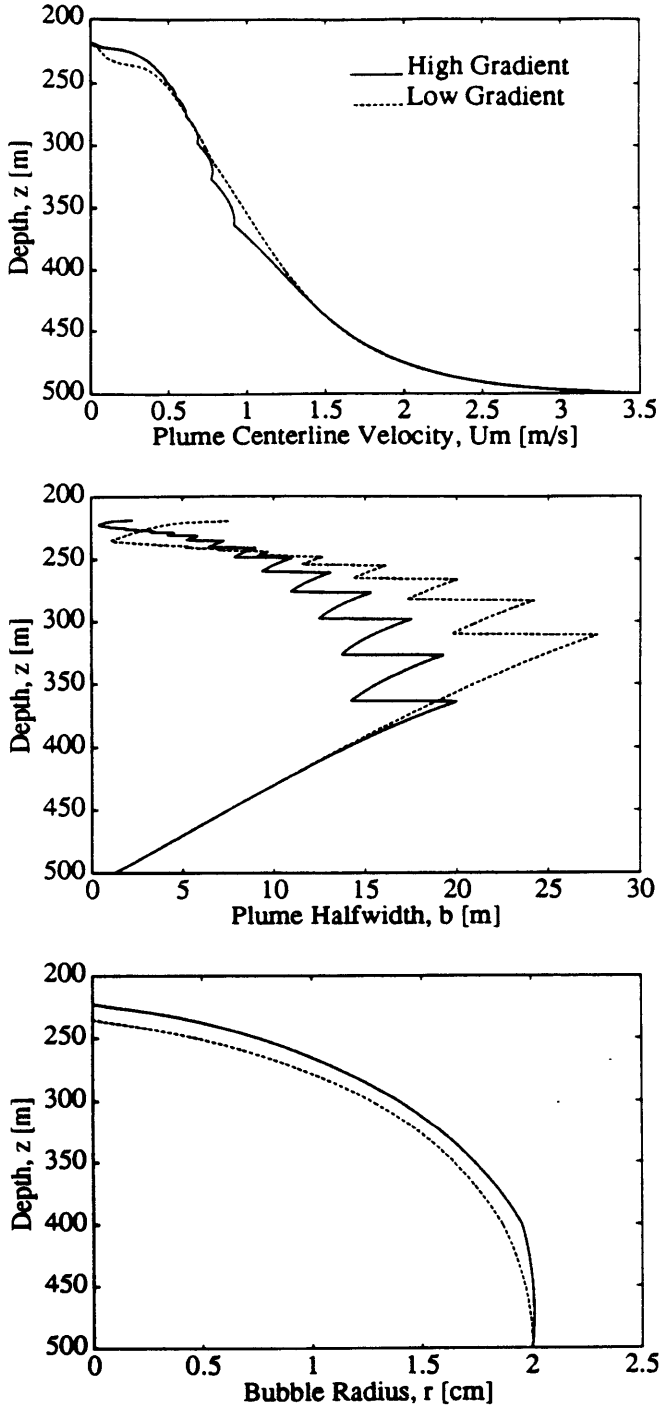

Figure A-11: Sensitivity to ambient profiles.

Appendix B

Computer Code

C code for numerical model:

```
/*****************************************************************************
******* BUBBLE PLUME MODEL FOR CO2 DISPOSAL          **********************
******* WITH MASS TRANSFER                        **********************
*******     DENSITY GRADIENT EFFECTS                **********************
*******     PHASE CHANGE                          **********************
*****************************************************************************/


#include <stdio.h>                                                          10
#include <math.h>
#include "utilities.h"

#define NVAR 4 /* r, deltarhow,b,um*/
#define NSTEP 1000
#define PI 3.14159


/*** Beginning of differential equation solver  ***/
void derivs(x,y,dydx,ro,so, alpha, lam1, lam2, Bflag, rflag)                20
float x, y[], dydx[];
double ro,so,  alpha, lam1, lam2;
int *Bflag, *rflag;
{
  double g, Mrel, gamma, dens, densdot, denssw, dpwds, deltdens, visc, D;
  double Cs, Cdm, Cm, Z, ub, K, Bpos, Bneg, qz, propvec[7];
  static double rD, qD, qrel, densrel, densref, massflux;

  g = 981.0;      /* gravitational accereration cm/s2 */
  Mrel = 133.0;   /* release CO2 mass flux kg/s */                          30
```

```
/*begin calculations*/

if(x == so) {
  properties(so, propvec); /* determine initial values*/
  densrel = propvec[2];    /* CO2 density kg/m3 */
  densref = propvec[0];    /* seawater density kg/m3 */
  qrel = Mrel/densrel;     /* release flow m3/s */
  massflux = Mrel;         /* release mass flux kg/s */                    40
}

properties(x, propvec); /*determine co2 and ocean properties at z */
denssw  = propvec[0];   /* seawater density kg/m3 */
dpwdz   = propvec[1];   /* seawater density gradient kg/m4 */
dens    = propvec[2];   /* co2 density kg/m3 */
densdot = propvec[3];   /* co2 density gradient kg/m4 */
Cs      = propvec[4];   /* co2 solubility kg/m3 */
D       = propvec[5];   /* molecular diffusion coefficient cm2/s */
visc    = propvec[6];   /* water viscosity cm2/s */                         50



/* z=x, r=y[1], delta rho w = y[2], b=y[3], Um=y[4] */

if(y[1]<=0.01) {  /* If r is near zero, indicate absence of bubbles */
  y[1] = 0.00001;
  *rflag = 1;
}
                                                                            60
if(y[2] > 1000000000.0)  /* Numerical limit to delta rho w */
  y[2] = 1000000000.0;

if(y[3] > 1000000000.0)  /* Numerical limit to b */
  y[3] = 1000000000.0;

if(y[4]<0.0)             /* Numerical limit to Um */
  y[4] = 0.00001;

if(y[3]<0.0)             /* Numerical limit to b*/                          70
  y[3] = 0.00001;


/* Solve for local properties */

Z = 0.217*2*y[1]*cbrt(g/(visc*visc));


if(so > 500.0) {                    /* if starts as liquid */
  if(x > 500.0) {                   /* liquid phase */                      80
    qs = qrel*(y[1]/ro)*(y[1]/ro)*(y[1]/ro);
    /*Clift Ub*/
    ub = 0.00711 * sqrt(g*2.0*y[1]*(denssw-dens)/denssw);
    /*Treyball Ub*/
    /*ub=0.2392*pow(((denssw-dens)/1000.0),0.28)*pow((dens/1000.0),-0.45);*/
    rD = y[1];
```

```
    qD = qz;
  }

  if(x <= 500.0 ) {                    /* change to vapor */                    90
    qrel = qD*5.156;
    ro = rD*1.728;
    qz = qrel*(y[1]/ro)*(y[1]/ro)*(y[1]/ro);
    ub = (1.0/100.0)*(2.355)*(108.4/Z + sqrt(Z/0.5479));/*m/s*/
  }
}


if(zo <= 500.0){                       /* if starts as vapor */
  qz = qrel*(y[1]/ro)*(y[1]/ro)*(y[1]/ro);                                      100
  ub = (1.0/100.0)*(2.355)*(108.4/Z + sqrt(Z/0.5479));/*m/s*/
}

/* WC K */
/*K = (4.917e-3)*sqrt(100.0*ub)/(sqrt(2.0*y[1])); */
/*Clift K for Cap Bubbles*/
K = 1.25*sqrt(sqrt(g*(denssw-dens)/denssw))*sqrt(D)/(sqrt(sqrt(2.0*y[1])));
/*Cussler K*/
/*K = 0.03919*cbrt((denssw-dens)/denssw);*/
Cm = ((qz/ (PI*y[3]*y[3]*lam1*lam1))/((y[4]/(1+lam1*lam1))+ub));                110
deltdens =  (densref-dens)/densref;
gamma = 1.0;


/*PEELING MODEL  */

Bpos = Cm*deltdens*lam1*lam1;
Bneg = y[2]*lam2*lam2/densref;
if((Bpos<Bneg) && (y[1]>0.01)){
  y[2] = 0.5*y[2];                                                              120
  y[3] = 0.707*y[3];   /*b*/
  /*y[4] = y[4]; /*U*/
  *Bflag = 1;
  massflux =  0.5*massflux + 0.5 * dens * qz;
}

/* CO2 Accumulation */
/*Cdm = 2 * (massflux - qz*dens) / (y[4] * PI * y[3] * y[3]);
printf("%10.6lf   %10.6lf \n", z, Cdm);*/
                                                                                130

/* solve differential equations */
/* dydx[1] = dr/dz, 2->dens, 3->b, 4->um */

dydx[1] = (K*Cs*0.85/(dens*(y[4]+ub))) - (y[1]*densdot/(3*dens)); /*cm/s*/
dydx[2] = -((1+lam2*lam2/(lam2*lam2))*dpwdz - (2*alpha*y[2]/y[3]));
dydx[3] = -((2*alpha) - (g*y[3]/(gamma*100.0*y[4]*y[4]))*
  (Cm*deltdens*lam1*lam1-(y[2]*lam2*lam2/densref)));
dydx[4] = -((2*g/(gamma*100.0*y[4]))*
            (Cm*deltdens*lam1*lam1-(y[2]*lam2*lam2/densref))-                   140
```

```
            (2*alpha*y[4]/y[3]));

} /* end of derivs()*/

/*PROPERTY FUNCTION*/
properties(z, densptr)
    double z, *densptr;
{
 double press, temp;
 int i;                                                          150
    /*  PROPERTIES FOR HIGH GRADIENT PROFILE */
    /*  z, denssw, dens, Cs, D, visc, P, T */
 static double densA[17][8] = {
  {  -1.0, 1025.15, 1.82, 1.74, 1.9e-5, 0.01, 1.00, 19.0 },
  { 100.0, 1025.15, 19.2, 16.2, 1.9e-5, 0.01, 10., 19.0 },
  { 200.0, 1025.41, 41.2, 30.4, 1.9e-5, 0.01, 20., 18.0 },
  { 300.0, 1025.68, 67.5, 42.1, 1.9e-5, 0.01, 30., 17.0 },
  { 400.0, 1025.94, 101.3, 50.6, 1.9e-5, 0.01, 40., 16.0 },
  { 500.0, 1026.2, 160.0, 54.4, 1.9e-5, 0.01, 50.0, 15.0 },
  { 500.0, 1026.2, 825.0, 55.4, 1.9e-5, 0.01, 50.0, 15.0 },      160
  { 600.0, 1026.46, 853.1, 60.0, 1.9e-5, 0.01, 60., 12.8 },
  { 700.0, 1026.72, 885.2, 60.0, 1.9e-5, 0.01, 70.,  10.6 },
  { 800.0, 1026.98, 912.0, 60.0, 1.9e-5, 0.01, 80.0,  8.4 },
  { 900.0, 1027.24, 934.6, 60.0, 1.9e-5, 0.01, 90,  6.2 },
  {1000.0, 1027.5,  953.5, 60.0, 1.9e-5, 0.01, 100., 4.0},
  {1200.0, 1027.52, 966.7, 60.0, 1.9e-5, 0.01, 120., 3.6},
  {1400.0, 1027.54, 981.0, 60.0, 1.9e-5, 0.01, 140., 3.2},
  {1600.0, 1027.56, 992.6, 60.0, 1.9e-5, 0.01, 160., 2.8},
  {2000.0, 1027.6, 1013.2, 60.0, 1.9e-5, 0.01, 200., 2.0},
  {3000.0, 1027.7, 1050.3, 60.0, 1.9e-5, 0.01, 300., 1.5}        170
 };

 i=0;
 while (z > densA[i][0])
  i++;

 /*denssw*/
 *densptr = ((densA[i][1]-densA[i-1][1])*(z-densA[i-1][0])/
        (densA[i][0]-densA[i-1][0])) + densA[i-1][1];
 /*dpwdz*/                                                        180
 *(densptr+1) = (densA[i][1]-densA[i-1][1])/(densA[i][0]-densA[i-1][0]);

 /*dens*/
 *(densptr+2) = ((densA[i][2]-densA[i-1][2])*(z-densA[i-1][0])/
        (densA[i][0]-densA[i-1][0])) + densA[i-1][2];

 /*densdot  */
  *(densptr+3) = (densA[i][2]-densA[i-1][2])/(densA[i][0]-densA[i-1][0]);

 /*Cs  */                                                         190
  *(densptr+4) = ((densA[i][3]-densA[i-1][3])*(z-densA[i-1][0])/
        (densA[i][0]-densA[i-1][0])) + densA[i-1][3];

 /*D*/
```

```
 *(densptr+5) = ((densA[i][4]-densA[i-1][4])*(z-densA[i-1][0])/
        (densA[i][0]-densA[i-1][0])) + densA[i-1][4];

 /*visc*/
 *(densptr+6) = ((densA[i][5]-densA[i-1][5])*(z-densA[i-1][0])/
        (densA[i][0]-densA[i-1][0])) + densA[i-1][5];                    200

 /*pressure*/
 press = ((densA[i][6]-densA[i-1][6])*(z-densA[i-1][0])/
        (densA[i][0]-densA[i-1][0])) + densA[i-1][6];

 /*temperature*/
 temp = ((densA[i][7]-densA[i-1][7])*(z-densA[i-1][0])/
        (densA[i][0]-densA[i-1][0])) + densA[i-1][7];

 } /*END OF PROPERTY FUNCTION*/                                           210


extern float **y, *x;
float **y=0, *xx=0;



/********* integrator driver *********************/

                                                                         220
void rkdrive(vstart, nvar, x1, x2, nstep, derivs, alpha, lam1, lam2)
int nvar, nstep;
float vstart[], x1, x2, alpha, lam1, lam2;
void (*derivs)();

{
 int i, k;
 float x,h;
 double ro,zo;
 float *v, *vout, *dv, *vector();                                        230
 void rk4(), error(), free_vector();

 v=vector(1,nvar);
 vout = vector(1, nvar);
 dv = vector(1, nvar);

 ro = vstart[1];
 zo = x1;

 for (i=1; i<=nvar; i++) {                                               240
  v[i]=vstart[i];
  y[i][1]=v[i];
 }
 xx[1]=x1;
 x=x1;
 h=(x2-x1)/nstep;
 for (k=1; k<=nstep; k++) {
  (*derivs)(x,v,dv,ro,zo, alpha, lam1, lam2);
```

```
    rk4(v, dv, nvar, x, h, vout, derivs, ro, zo, alpha, lam1, lam2);
    if (x+h == x) nrerror("Step size too small in routine RKDRIVE");
    x += h;
    xx[k+1]=x;
    for (i=1; i<=nvar; i++) {
      v[i] = vout[i];
      y[i][k+1] = v[i];
    }
  }
  free_vector(dv,1,nvar);
  free_vector(vout,1,nvar);
  free_vector(v,1,nvar);
}   /** end of RKDRIVE  **/



/* Fourth Order Runge-Kutta Numerical Integrator */

void rk4(y,dydx,n,x,h,yout,derivs,ro,zo, alpha, lam1, lam2)
float y[], dydx[], x, h, yout[];
void (*derivs)();
double ro, zo, alpha, lam1, lam2;

{
  int i, Bflag, rflag;
  float xh, hh, h6, *dym, *dyt, *yt, *vector();


  dym = vector(1,n);
  dyt = vector(1,n);
  yt = vector(1,n);
  hh = h*0.5;
  h6 = h/6.0;
  xh = x + hh;
  for (i=1; i<=n; i++)  yt[i]=y[i]+hh*dydx[i];
  (*derivs)(xh, yt, dyt, ro, zo, alpha, lam1, lam2, &Bflag, &rflag);
  for (i=1; i<=n; i++) yt[i]=y[i]+hh*dyt[i];
  (*derivs)(xh, yt, dym, ro, zo, alpha, lam1, lam2, &Bflag, &rflag);
  for (i=1; i<=n; i++) {
    yt[i] = y[i] + h*dym[i];
    dym[i] += dyt[i];
  }
  (*derivs)(x+h, yt, dyt, ro, zo, alpha, lam1, lam2, &Bflag, &rflag);
  for (i=1; i<=n; i++)
    yout[i] = y[i] + h6*(dydx[i]+dyt[i]+2.0*dym[i]);


  /* limiters and modifiers */

  if(rflag == 1)
    yout[1] = 0.0;
```

```
  /* peeling model */
  if((Bflag == 1) && (rflag != 1)) {
    yout[2] = 0.5*yout[2];
    yout[3] = 0.707*yout[3];    /*b*/
    /*yout[4] = yout[4];   /*U*/
  }

  if( (500.0 - h >= x) && (x > 500.0) ) {    /*** phase  change to vapor ***/
      y[1] = 1.728*y[1];
      yout[1] = y[1];
    }
  free_vector(yt,1,n);
  free_vector(dyt,1,n);
  free_vector(dym,1,n);

} /** end of RK4 **/


main()  /* Beginning of main */
{
  FILE *fpws, *fopen();
  int j;
  float x1, x2, *vstart, alpha, lam1, lam2;
  vstart = vector(1, NVAR);
  xx = vector(1, NSTEP+1);
  y = matrix(1, NVAR, 1, NSTEP+1);

  printf("Input initial depth [m] :  ");
  scanf("%f", &x1);
  x2 = 0.0;

  printf("\nInput ro [cm] :  ");
  scanf("%f", &vstart[1]);

  vstart[2] = 0.0; /*delta pw*/

  printf("\nInput bo [m] :  ");
  scanf("%f", &vstart[3]);
  printf("\nInput umo [m/s] :  ");
  scanf("%f", &vstart[4]);

  printf("\nInput entrainment coefficient, alpha:  ");
  scanf("%f", &alpha);
  printf("\nInput CO2 volume spreading ratio, lam1:  ");
  scanf("%f", &lam1);
  printf("\nInput water density spreading ratio, lam2:  ");
  scanf("%f", &lam2);

   /* call integrator */
  rkdrive(vstart, NVAR, x1, x2, NSTEP, derivs, alpha, lam1, lam2);

   /* output */
  fpws = fopen("plumeout", "w");
```

```
  for(j=1; j<=NSTEP+1; j++)
   {
    /*y[1][i] = r  y[2][i]=deltap y[3][i]=b y[4][i]=Um*/
    if (y[4][j] > 0) {                                                    360
        fprintf(fpwz, "%f    %f   %f   %f   %f \n",
                xx[j], y[1][j], y[2][j], y[3][j], y[4][j]);
    }
   }
  printf("\n Output in file:  plumeout.  \n");

  free_matrix(y,1,NVAR,1,NSTEP+1);
  free_vector(xx,1,NSTEP+1);
  free_vector(vstart,1,NVAR);
  fclose(fpwz);                                                           370
} /*end of main*/
```